



# Validation of a practice-oriented floor spectra formulation through actual data from the 2016/2017 Central Italy earthquake

Stefania Degli Abbatì<sup>1</sup> · Serena Cattari<sup>1</sup> · Sergio Lagomarsino<sup>1</sup>

Received: 15 February 2022 / Accepted: 12 August 2022 / Published online: 30 August 2022  
© The Author(s) 2022

## Abstract

Analytical expressions for the floor spectra evaluation play a key role in the correct definition of the seismic input induced to non-structural elements or local mechanisms in existing buildings. They have to be able properly assessing the possible amplification phenomena, but also correctly describing the effects of nonlinearities due to structural damage. Due to the complexity of such phenomena, data on existing structures hit by earthquakes constitute a precious source for a better understanding of the topic and the validation of analytical expressions. In this framework, the paper aim is twofold. On one hand, it evaluates the entity of seismic amplification through experimental evidences from *in-situ* measurements on two existing monitored unreinforced structures. On the other hand, it presents the application on them of an analytical expression for the floor spectra already developed by the Authors. The case-studies are the former courthouse of Fabriano (Ancona, Italy) and the Pizzoli's town hall (L'Aquila, Italy). They were both hit by the 2016/2017 earthquake in Central Italy and are permanently monitored by the Italian seismic monitoring system of the Italian Department of Civil Protection. With the aim of validating the above-mentioned expression, the paper shows the comparison between experimental and analytical floor spectra for various minor events and mainshocks of the Central Italy earthquake. Since the two case-studies exhibited different damage levels (from slight to moderate, respectively), the comparison allowed us to verify the reliability of the expression both in the pseudo-elastic and moderate nonlinear fields.

**Keywords** Floor spectra · Masonry · Buildings permanently monitored · Seismic analysis · Nonstructural elements

---

✉ Stefania Degli Abbatì  
stefania.degliabbati@unige.it

Serena Cattari  
serena.cattari@unige.it

Sergio Lagomarsino  
sergio.lagomarsino@unige.it

<sup>1</sup> DICCA, Department of Civil, Chemical Environmental Engineering, University of Genova, Via Montallegro 1, 16145 Genoa, Italy

## 1 Introduction

In the seismic assessment of existing buildings, a crucial and tricky aspect is the proper definition of the seismic input to be used for the verification of acceleration-sensitive non-structural elements or local mechanisms placed atop masonry buildings. Traditionally, the approaches recommended by Codes (*e.g.* Eurocode 8, 2004; ASCE/SEI 7-10, 2010; New Zealand Code, 2017; Commentary of the Italian Technical Code, 2019) define the seismic action in terms of floor spectra that, as known, assume as licit the decoupling between main and secondary structures (Chen and Soong, 1988; Muscolino, 1991).

The seismic input on an element housed at a certain level of a building is greatly influenced by the properties of both the primary structure and the element itself, that act as two filters connected in series. Due to this filtering effect, the characteristics of floor acceleration motions (*i.e.*, the induced motions at the base of the element) are markedly different from those of typical ground accelerations. The main parameters affecting the phenomenon are the characteristics of the ground motion (amplitude, frequency content and duration—Rodriguez et al. 2021), the dynamic response of the primary structure, the lateral load resisting system, the floor level and the level of nonlinearity of both primary structure and nonstructural element (Anajafi et al. 2019; Kazantzi et al. 2020a, 2020b). Moreover, many additional parameters, such as diaphragm flexibility, torsional responses and also uncertainties in the inelastic behavior, can further amplify the seismic demands on nonstructural elements (Anajafi and Medina, 2019; Derakhshan et al. 2020). This research field is topical; thus, many numerical and experimental studies are available in literature, whose main findings are briefly summarized below.

Baggio et al. (2018) compared the ground with the floor acceleration time-histories computed in a Finite Element (FE) model of a complex masonry building (*i.e.* the Palazzo dei Musei in Modena, Italy). This comparison showed an important amplification phenomenon; moreover, the acceleration floor spectra numerically evaluated showed that the host building acts as a filter, by amplifying the frequency content of the seismic input in correspondence of the structural fundamental period. Analogous results were also experimentally observed in many shake-table campaigns (*e.g.* Senaldi et al. 2014; Magenes et al. 2014; Beyer et al. 2015; Senaldi et al. 2020). Furthermore, the results obtained by Baggio et al. (2018) confirmed that, in case of complex structures, the simplified expressions typically suggested by Codes for the evaluation of the fundamental period are not adequate.

A reduction in the acceleration amplification with an increasing nonlinear behavior was documented for unreinforced masonry (URM) buildings, *e.g.* in the numerical studies by Menon and Magenes (2011a) or in the experimental studies by Bothara et al. (2010) and Beyer et al. (2015). In the two latter works, the dynamic identification performed after each test highlighted that the fundamental frequencies gradually reduced when the prototype was exposed to excitations of increasing severity, while at the same time the structural damping increased; moreover, the transfer functions for the eaves level response acceleration computed by Bothara et al. (2010) showed a clear shift in frequency from a higher to a lower value during the shakings. This shift was ascribed by the authors to the decreasing of stiffness due to cracking but also due to inelastic rocking behavior of some piers in the prototype. Derakhshan et al. (2020) reviewed empirical data from nine buildings obtained from the Centre for Engineering Strong Motion Data (CESMD 2019) for a qualitative evaluation of the effects of diaphragm flexibility. The building height of the considered samples varied from 6.7 to 12.6 m, while the horizontal diaphragms were made of timber sheathing on timber joists and/or steel framing. The acceleration amplification at the top

of the walls ( $Amp_w$ ) and at the mid-span of the diaphragms in short direction ( $Amp_d$ ) was plotted as a function of the peak ground acceleration (PGA). The results showed an overall decrease in the amplification with an increase in earthquake intensity; a lack of correlation between amplifications and building height was instead found, mainly attributed by the authors to the diaphragm effects which have overshadowed the effect of building height on wall accelerations. Moreover, the large  $Amp_d/Amp_w$  ratio highlighted the importance of considering diaphragm vibration effects when amplifying acceleration input to nonstructural components. Finally, the results of pushover and incremental dynamic analyses carried out through equivalent frame (EF) models of four building typologies showed that the accelerations in buildings with flexible diaphragms are amplified by up to 3 when compared to the case of buildings with rigid diaphragms.

Another important parameter that can affect the floor spectra is the torsional response of the main building. For example, a study on instrumented buildings in California (USA) showed that the torsional responses of the supporting structure and/or the in-plane flexibility of floor diaphragms can increase by not negligible factors the seismic-induced force demands on elastic acceleration-sensitive nonstructural components (Anajafi and Medina, 2019).

Available results of experimental tests are no doubt very useful to investigate the amplification phenomenon because they guarantee a detailed knowledge of both prototype and input. At the same time, numerical analyses allow the analyst to parametrically quantify the effects on floor accelerations and floor spectra of many uncertainties, which are inherent in the characteristics of ground excitation, primary structure and nonstructural elements themselves. However, experimental or numerical prototypes necessarily imply simplifications when compared to actual structures (due to lab or computational limitations, instrumentation needs, etc.). Thus, accurate data on existing structures hit by earthquakes are very valuable to understand the complexity of the phenomenon and to validate the analytical expressions proposed in literature. The latter is a research field that gained increasing interest in the last years due to its important repercussion on the engineering practice (e.g. Menon and Magenes, 2011a, b; Sullivan et al. 2013; Calvi and Sullivan, 2014; Petrone et al. 2015; Vukobratović and Fajfar, 2016, 2017; Lucchini et al. 2017; Surana et al. 2018; Degli Abbatì et al. 2018; Merino et al. 2019; Di Domenico et al. 2021).

Within this context, the paper firstly presents the post-processing of some recordings provided on two URM buildings (Sect. 2) in order to deepen and physically understand the amplification phenomenon (Sect. 3). The two buildings are the former courthouse of Fabriano (Ancona, Italy) and the Pizzoli's town hall (L'Aquila, Italy). They were selected within the aims of the ReLUIIS project funded by the Department of Civil Protection (DPC, Cattari et al. 2019) because they are permanently monitored by the Italian seismic monitoring network (Dolce et al. 2017), hereinafter briefly named as "OSS", an acronym which stands for the Italian "*Osservatorio Sismico delle Strutture*". The monitoring system includes accelerometers at different levels plus a three-axial sensor at the foundation, which measures the seismic excitation applied to the structure. Records from various mainshocks, secondary seismic events and ambient noise are available.

Secondly, the data from the monitoring system are used to validate the analytical expression proposed in 2018 by the Authors for the floor spectra estimate (Degli Abbatì et al. 2018). This expression allows evaluating the floor spectra in different points of the building and at different levels by considering the contribution of the more relevant modes, properly combined (Sect. 4). For the aim of the validation, the comparison of the experimental floor spectra (*i.e.* evaluated from the recorded accelerations) with the analytical ones is presented in the paper for the two above-mentioned case-studies (Sects. 5 and 6). Both were

hit by the 2016/2017 Central Italy earthquake exhibiting from negligible to moderate damage levels; thus, the comparison allowed us to validate the expression both in the pseudo-elastic field and for a slightly higher level of nonlinearity.

## 2 Dataset of monitored URM buildings hit by the Central Italy earthquake

The examined case-studies are two URM buildings built in the first half of '90 s and characterized by external masonry façades with openings generally aligned and quite stiff diaphragms. Both are regular in elevation but with an irregular in-plan configuration.

The former courthouse of Fabriano (Fig. 1a) is a quite complex structure with four storeys (one is partially underground) and a T-shaped plan; the total height is equal to 16.8 m and the average storey's area is about 1220 m<sup>2</sup>. The walls are made of regular masonry of three typologies (stone masonry, solid-brick masonry and stone masonry with an external brick face), while the horizontal diaphragms are of four typologies: diaphragms with H steel beams, small brick vaults and a reinforced concrete (RC) slab (equivalent shear stiffness equal to  $G_{eq} = 7.52 \times 10^{11} \text{ Nm}^{-1}$ ); diaphragms with H steel beams, hollow clay blocks and a RC slab ( $G_{eq} = 7.52 \times 10^{11} \text{ Nm}^{-1}$ ); diaphragms with H steel beams, corrugated sheet and a RC slab ( $G_{eq} = 1.18 \times 10^{12} \text{ Nm}^{-1}$ ); diaphragms with  $\Omega$ -shape steel elements and timber flooring ( $2.45 \times 10^{10} \text{ Nm}^{-1}$ ). In some smaller areas, where a higher stiffening effect was expected, the equivalent shear stiffness in the numerical model shown in Fig. 3 was increased of one order of magnitude. Some strengthening interventions were provided in 1999 after the Umbria and Marche

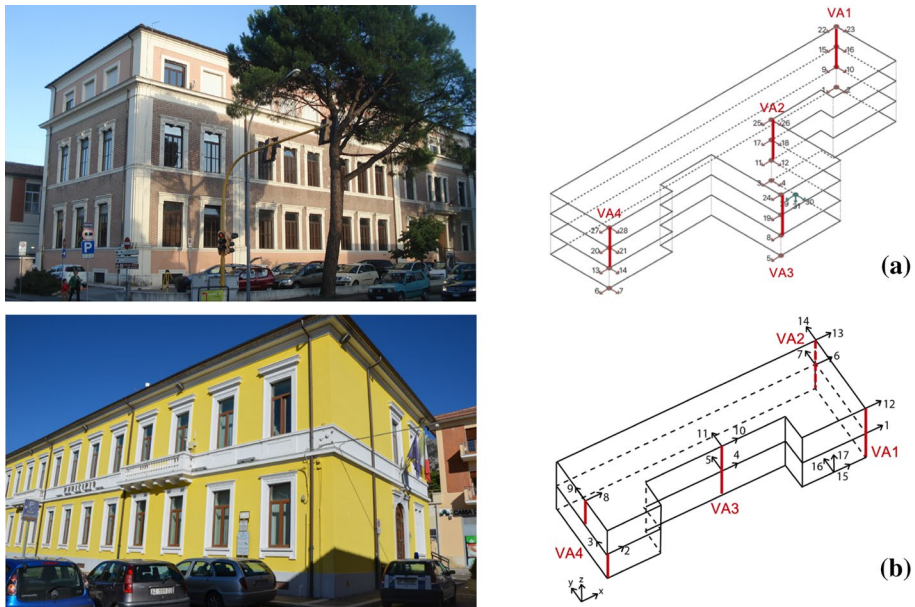


**Fig. 1** Pictures (on the left) and sensors layout (on the right) in the two examined case-studies: **a** the former courthouse of Fabriano, **b** the Pizzoli's town hall

earthquake (1997) in order to restore the damage and improve the building seismic response. The most significant ones were: replacement of the original stairwell with a RC one, disconnected from the main building through a seismic joint; strengthening interventions of the vertical walls with reinforced plaster; local interventions on horizontal floors (sometimes replaced, sometimes reinforced with an additional RC slab); strengthening of the roof by means of steel X-bracing; improvement of the wall-to-wall connections through reinforced riveting. The identification of the main structural interventions together with more data on geometry and construction details are illustrated in Cattari et al. (2021).

The Pizzoli's town hall (Fig. 1b) presents a C-shaped plan, whose dimensions are about  $38 \times 12.5$  m. The building has two levels, a basement and a non-habitable attic with a pavilion roof, composed of RC joists and hollow clay units and a 3 cm thick slab. The total height of the building is approximately 8.6 m. The walls are made of regular stone masonry and the horizontal floors consist of small iron beams and hollow clay units capped with a RC slab ( $G_{eq} = 2.74 \times 10^8 \text{ Nm}^{-1}$ ). More data about geometry and construction details can be found in Cattari and Magenes (2022) and Degli Abbatì et al. (2022).

Both case-studies are instrumented by OSS as strategic buildings with a permanent accelerometric monitoring system that includes force-balance accelerometers (in most cases bi-axial) placed on the various floors plus a three-axial sensor at the foundation, which records the seismic excitation applied to the structure. The latter instrument is important to evaluate the amplification effects on floor accelerations with respect to the ground excitation. The working range of accelerometers is set to account for both low vibrations tremors and strong-motion earthquakes, with accelerations from  $10^{-4}$  to 2 g. The main characteristics of the employed sensors are reported in Dolce et al. 2017. The sensor layout on the two examined case-studies is shown in Fig. 1 (on the right), which identifies also the sensors placed along the same vertical alignment (VA), colored in red.

The buildings were hit by the 2016/2017 Central Italy earthquake and exhibited very different levels of damage. According to EMS-98 (Grünthal et al. 1998), negligible to slight damage occurred on the Fabriano courthouse, while the Pizzoli's town hall, mostly hit by the mainshock of January 18, 2017, suffered a moderate damage. In particular, Fig. 2 shows the damage detected on the Pizzoli's town hall after an *in-situ* survey made by the ReLUIS research group (Cattari et al. 2019): such damage was mainly concentrated in masonry piers at both levels and it was characterized by the presence of both pseudo-horizontal cracks (mainly associated with a flexural mode) and diagonal cracks (associated to a shear failure mechanism).

Starting from the data on geometry, construction details and materials available from OSS, it was possible to set up a numerical model of each structure (Fig. 3a). The models were developed with the Tremuri software that is based on the EF modelling approach (Lagomarsino et al. 2013) and they were calibrated and validated in previous studies [see Degli Abbatì et al. (2022) for the Pizzoli's town hall and Cattari et al. (2021) for the former courthouse of Fabriano]. The EF approach considers only the in-plane behavior of masonry walls and concentrates the deformability and the nonlinear behavior into specific portions of URM walls, namely piers (vertical elements) and spandrels (masonry beams that connect piers). This approach is reliable when the box behavior is guaranteed. This assumption is licit for both the case-studies, as demonstrated by the exhibited post-earthquake damage and deduced from the analysis of the construction details.

The numerical models were calibrated in the elastic field using as target some dynamic identifications available in literature and performed with the ambient vibration data acquired by the OSS accelerometers, with a sampling frequency of 250 Hz. In particular:



**Fig. 2** Damage survey detected on the Pizzoli's town hall during the *in-situ* inspections performed after the mainshock of 18/01/2017—figure adapted from Degli Abbati et al. 2022 (local severe damage is in red)

- For the courthouse of Fabriano, the target of the calibration process was the dynamic identification performed under operational conditions with the “stochastic subspace identification covariance-driven” (SSI-Cov) algorithm and using the ambient noise of December 7, 2016 (Cattari et al. 2021—AN in Table 1).
- For the Pizzoli's town hall, the target was the dynamic identification provided by Sivori et al. (2021) performed using the ambient vibration data acquired on October 1, 2016 for one hour and employing the frequency domain decomposition technique with a frequency resolution of 0.05 Hz (Degli Abbati et al. 2022).

The results of the elastic calibration of the numerical models are illustrated in Fig. 3b and c where a comparison between the measured (labeled “experimental”) and numerical data (labeled “numerical”) is reported in terms of frequencies (Fig. 3b) and Modal Assurance Criterion (MAC) indexes (Fig. 3c—Allemange and Brown 1982), respectively. The latter provides a measure of the correlation between numerical and experimental mode shapes: the closer the numerical values to the experimental ones, the more MAC indexes tend to 1. The frequencies errors are expressed in percentage and reported in brackets on the X-axis of the histograms of Fig. 3b. From these results, it is possible to see that the calibrated models show a good fitting with the experimental target both in terms of frequencies (with errors on the first four modes lower than 7% for both the case-studies) and mode shapes (with MAC index on the first four modes higher than 0.63 and 0.95 for the former courthouse of Fabriano and the Pizzoli's town hall, respectively). After the model calibration, nonlinear dynamic analyses were performed on the models, using as input the accelerograms recorded during the Central Italy earthquake by the sensors placed at the base of the buildings. The comparison between simulated and recorded response performed at global and local scales (*e.g.* in terms of hysteretic shear-displacement curves, damage pattern, accelerations on sensors and floor spectra) allowed also the model validation in the nonlinear range. For further details on model calibration and validation, the interested



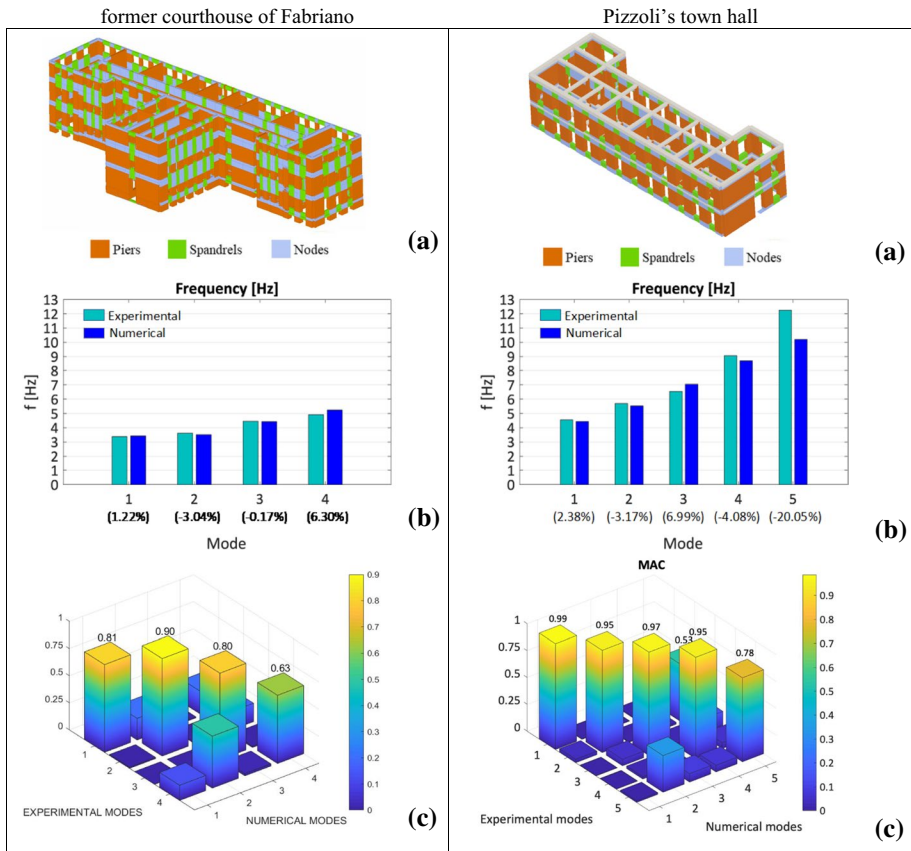


**Fig. 3** For the two case-studies: **a** Calibrated EF models. **b** Comparison between measured and numerical frequencies (errors expressed on the X-axis in brackets). **c** Comparison in terms of MAC indexes

**Table 1** Frequencies [Hz] identified during the seismic events (table adapted from Cattari et al. 2021)

Modes	Event ID									
	E1	SE1	E2	E3	SE2	E4	SE3	AN	E5	SE4
1	3.20	–	3.30	2.36	–	2.40	–	3.37	2.81	3.16
2	–	3.91	–	–	3.46	2.81	3.17	3.60	3.23	3.52
3	4.31	4.78	4.24	3.91	4.34	3.48	4.29	4.44	4.26	4.50
4	4.63	5.33	4.82	4.05	4.82	3.99	4.58	4.91	4.90	5.06
5	–	5.53	–	–	–	4.37	4.88	5.39	5.09	5.42
6	5.12	5.94	–	–	5.37	–	5.00	5.61	–	5.52
7	5.82	6.83	–	–	–	–	–	6.61	5.93	6.87
8	6.63	–	6.79	–	6.89	5.74	6.26	7.51	6.51	–

Abbreviations: *E* mainshock, *SE* secondary event, *AN* ambient noise

E1: 24/08/2016 01:36; E2: 26/10/2016 17:10; E3: 26/10/2016 19:18; E4: 30/10/2016 06:40; E5: 18/01/2017 10:14

SE1: 08/10/2016 18:11; SE2: 28/10/2016 13:56; SE3: 03/11/2016 00:35; SE4: 03/02/2017 05:40; AN: 07/12/2016 15:14

readers may refer to Cattari et al. (2021) and Degli Abbati et al. (2022). In the following, these models are used to assess the parameters useful to apply the analytical expression adopted for the computation of floor spectra.

### 3 Physical interpretation of the amplification phenomenon for the examined case-studies

Figure 4 shows some post-processing of the recordings acquired by the permanent monitoring system on the two buildings presented in Sect. 2.

In particular, Fig. 4a,b compares the response spectrum recorded at the base (dotted plot) with the floor spectra obtained from some sensors placed along the same VA at increasing height (thicker plot lines). All response spectra are evaluated with a 5% damping. In particular, the numbers of sensors are: 30, 10, 16 and 23 in the Y direction for the former Fabriano courthouse (VA1 in Fig. 1a); 15, 1 and 12 in the X direction for the Pizzoli's town hall (VA1 in Fig. 1b). The recordings refer to the two seismic events which mainly hit the structures during the Central Italy earthquake, *i.e.*: the second shake of the main event of 26/10/2016, for the Fabriano courthouse; the mainshock of 18/01/2017, for the Pizzoli's town hall. This comparison clearly highlights the amplification phenomenon, which is in both cases more pronounced at the top and in correspondence of the fundamental periods in the direction of interest, that are:  $T_{I,Y}=0.424$  s, for the former Fabriano courthouse (this is the fundamental period in the Y direction and corresponds to mode 1 in Fig. 5);  $T_{I,X}=0.197$  s, for the Pizzoli's town hall (this is the fundamental period in the X direction and corresponds to mode 3 in Fig. 12). The values of these periods were identified through an input–output analysis using the time-histories recorded during these two mainshocks in Cattari et al. (2021) and in Cattari et al. (2018), for the former courthouse and the town hall, respectively. These values are higher than those identified under operational conditions because it was observed that frequencies decrease systematically with increasing amplitude of the shaking at base for all the main structural modes (Michel and Guéguen, 2010; Lorenzoni et al. 2019; Cattari et al. 2021; Martakis et al. 2022). Moreover, the floor spectra plot in Fig. 4b,c) for the Pizzoli's town hall have a second peak around  $T=0.08\text{--}0.09$  s which could be related to a higher mode, experimentally identified by Sivori et al. (2021) at 12.25 Hz.

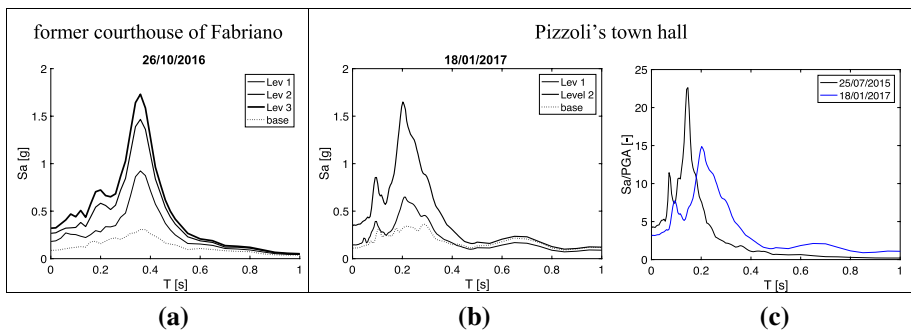


**Fig. 4** Amplification phenomenon recorded by the monitoring system on: **a** the former courthouse of Fabriano (main event of 26/10/2016–19:18), and **b** the Pizzoli's town hall (main event of 18/01/2017). **c** Effects of nonlinearity on the floor spectra shape for the Pizzoli's town hall



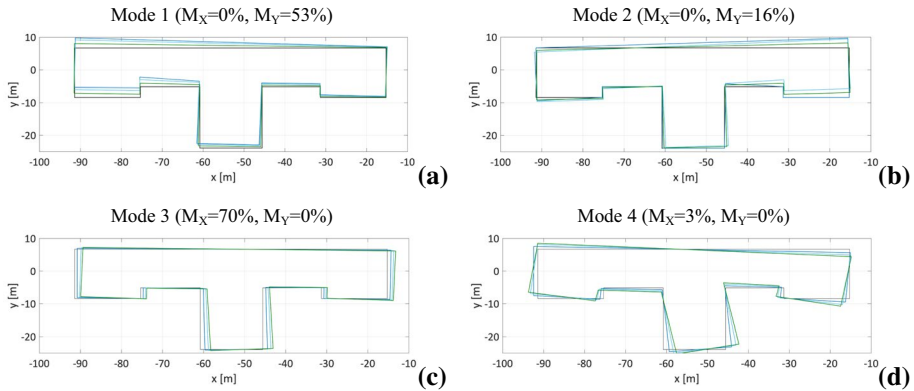


**Fig. 5** Numerical mode shapes of the former courthouse of Fabriano (each color refers to a different story): **a** mode 1, **b** mode 2, **c** mode 3, **d** mode 4

For the Pizzoli’s town hall, Fig. 4c) shows the effects of the nonlinearity on the floor spectra normalized to the *PGA*. To this aim, the floor spectrum obtained after a minor event (in black) is compared with that derived from the mainshock of 18/01/2017 (in blue). This comparison shows that the nonlinearity due to the exhibited damage determines an elongation of the resonance period and a reduction of the spectral amplification peak. This is clear from Fig. 4c), where it is possible to see: a peak of spectral acceleration around  $T_{l,x}=0.153$  s, when the floor spectrum is obtained before the Central Italy earthquake (this period corresponds to mode 3, as identified under operational condition—Fig. 12); a lower peak around an elongated period  $T_{l,x}=0.197$  s, when the floor spectrum is evaluated during the mainshock of 18/01/2017. This trend is the same experimentally observed from the shaking table tests mentioned in Sect. 1 (see for example Beyer et al. 2015), even if it can be recognized in a less systematic way from *in-situ* measurements on existing buildings. This is due to different reasons, *e.g.*: recorded floor spectra come from different seismic events, while the same seismic input is scaled up to inducing increasing damage in the prototype tested on shaking table; buildings are more complex than experimental prototypes and they are affected by more uncertainties; the shaking table campaign is designed, so the different parameters affecting the floor spectra can be investigated independently. All these reasons contribute to a trickier interpretation of the amplification phenomenon starting from the analysis of *in-situ* measurements.

#### 4 Basics of the considered practice-oriented floor spectra formulation

The expression applied in this paper to analytically compute the floor spectra was the one originally proposed by the Authors in Degli Abbati et al. (2018). The interested reader can refer to the original publication for all the details, while the main basics of the proposal are briefly recalled below.

The expression follows a floor spectrum approach, that is based on the simplified assumption to neglect the dynamic interactions between building and secondary elements (*i.e.* nonstructural elements or local mechanisms). It was verified that this assumption is licit when the secondary element has a negligible mass with respect to the one of the building (Degli Abbati et al. 2018; Muscolino, 1991). The expression

evaluates the seismic demand induced on secondary elements in terms of floor spectra in different points of the building and at different levels, by properly combining the contribution of the relevant modes. The expression is easy-to-use, because it depends on few parameters, that are: the seismic input at the base, expressed in terms of response spectrum; the main dynamic parameters of the selected modes; the damping features of building and secondary element to be verified. These data can be directly obtained from a numerical model of the structure or by applying simplified expressions available in literature and codes (Degli Abbatì et al. 2017, 2021). The explicit dependence of the analytical expression on the mode shapes is a key feature because it allows implicitly to account for the effects of diaphragm flexibility or torsion, that are not taken into account in some code proposals (Sect. 7).

Equation (1) summarizes the used expression, which gives the acceleration floor spectra at the level  $Z$  of the building, as:

$$S_{a,Z}(T, \xi) = \sqrt{\sum_{k=1}^N S_{aZ,k}^2(T, \xi)} \quad (\geq S_a(T)\eta(\xi) \text{ for } T > T_1) \tag{1}$$

where  $Z$  is the level where the secondary element of period  $T$  and damping  $\xi$  is placed,  $S_a(T)$  is the acceleration response spectrum of the ground motion,  $N$  is the number of considered modes and  $S_{aZ,k}(T, Z)$  is the contribution of the  $k$ th mode that is given by:

$$S_{a,Z}(T, \xi) = \begin{cases} \frac{AMP_k PFA_{Z,k}}{1+[AMP_k-1]\left(1-\frac{T}{T_k}\right)^{1.6}} & T \leq T_k \\ \frac{AMP_k PFA_{Z,k}}{1+[AMP_k-1]\left(\frac{T}{T_k}-1\right)^{1.2}} & T > T_k \end{cases} \tag{2}$$

In particular, in Eq. (2):

- $PFA_{Z,k}$  is  $k$ th peak floor acceleration that depends on the modal parameters of the building in terms of natural periods ( $T_k$ ), modal participation coefficients ( $\Gamma_k$ ) and modal shapes ( $\Phi_k(XYZ)$ ) and its viscous damping  $\xi_k$ . Furthermore, it depends on the ground spectrum  $S_a(T_k)$  calculated in correspondence of the structure natural period  $T_k$  and properly reduced through the damping correction factor  $\eta(\xi_k)$ :

$$PFA_{Z,k} = S_a(T_k)\eta(\xi_k)|\Gamma_k\phi_k|\sqrt{1+4\xi_k^2} \tag{3}$$

- $AMP_k = f_k f_s$  is an amplification factor of the  $PFA_{Z,k}$ , defined by two contributions:  $f_k$  that depends only on the viscous damping of the building, and  $f_s$  that depends only on the viscous damping of the secondary element. The expressions proposed to calculate  $f_k$  and  $f_s$  are:

$$f_k = \xi_k^{-0.6} \tag{4}$$

$$f_s = \eta(\xi) = \sqrt{\frac{0.1}{0.05 + \xi}} \geq 0.55 \tag{5}$$

The damping  $\xi_k$  allows the expression to account for the regime in which the building works, if still pseudo-elastic or nonlinear. In particular, it is possible to consider its

nonlinear behavior through an equivalent linear system, taking into account the period elongation and an increased damping  $\xi_k$  of all the modes for which the nonlinearity occurs.

#### 4.1 Criteria adopted for the validation of the floor spectra formulation

In order to validate the expression recalled at Sect. 4, the experimental floor spectra obtained from the monitoring system were compared with the analytical ones. While the first ones were evaluated through a step-by-step integration of the floor acceleration time histories recorded by the sensors at each storey, the second ones were computed by using the parameters defined hereinafter:

- The ground response spectrum calculated in correspondence of the structural natural periods—namely,  $S_a(T_k)$ —was determined from the accelerations applied to the structure and recorded by the three-axial sensor at the base. In particular, in both case-studies,  $S_a(T_k)$  was computed as the integral in a proper range of periods around  $T_k$ , assumed equal to  $T_k \pm 0.06$  s. This was done in order to reduce the sensitivity to the estimation of  $T_k$  that is usually present when the floor spectra are computed starting from a response spectrum derived from an actual record. Indeed, the latter has an irregular shape due to the presence of peaks and valleys (see for example the response spectra at the foundation in Fig. 4a,b); thus, the value of  $S_a(T_k)$  can differ a lot if computed in correspondence of a peak or a valley.
- All the structural dynamic parameters were directly obtained from a modal analysis performed on the calibrated EF models, once selected the number of modes considered representative to describe the structural response. This is coherent with the procedure typically followed in the engineering practice, where monitored data aren't usually available, and the practitioner evaluates the necessary parameters from a numerical model.
- The damping factor of the building  $\xi_k$  associated to each mode was instead evaluated following a two-step procedure. Firstly (*step 1*), the structural damping was obtained from the experimental data in order to guarantee the best fitting in terms of peaks between analytical and recorded floor spectra. In particular, it was obtained for each sensor and on the dominant mode. The dominant mode is the one characterized by the major contribution in terms of the product  $P$  [Eq. (6)] normalized to the maximum one (hereinafter defined  $P_{norm}$ ). Then (*step 2*), it was determined only a value for each mode, evaluated as the mean of the damping factors obtained in the previous step.

$$P = S_a(T_k) |\Gamma_k \phi_k(X, Y, Z)| \quad (6)$$

- Finally, a damping factor  $\xi$  equal to 5% was assumed in all cases, since the aim of the paper was to evaluate the seismic demand induced to a secondary element assumed to be still in the elastic phase.

## 5 Application to the former courthouse of Fabriano

### 5.1 Assessment of data used as input for the analytical computation of floor spectra

This section presents how the parameters necessary to analytically compute the floor spectra were evaluated for the former Fabriano's courthouse.

The ground response spectrum was computed from the accelerations recorded by the sensors n.29 and n.30 placed at the building foundation (Fig. 1a). In particular, the recordings of the secondary event of 19th April 2014 (with  $PGA_X=0.00126$  g and  $PGA_Y=0.00136$  g) and of the mainshock of 26th October 2016—19:18 ( $PGA_X=0.082$  g;  $PGA_Y=0.088$  g) were used.

The contribution of the first eight modes was considered, since the building has a quite irregular in-plan configuration and it is expected that the dynamic response could be affected also by the presence of higher modes. Figure 5 shows the numerical mode shapes of the first four modes, that are the ones activating the most significant participant mass (overall close to 70%). In particular, the first ( $T=0.293$  s) and second ( $T=0.286$  s) modes activate the transversal response of the two wings in the Y direction, the third mode ( $T=0.226$  s) is in the X direction, while the fourth mode ( $T=0.191$  s) is torsional.

In order to apply the expression presented in Sect. 4, it was necessary to compute the periods, the mode shapes and the participation coefficients of each mode, assumed as described below.

As far as the periods concern:

- For the floor spectra evaluation of the secondary event, the periods were the numerical ones obtained from the modal analysis performed on the model calibrated in the elastic field. As already clarified in Sect. 2, the experimental target for the calibration was the ambient noise of December 7, 2016 (namely, AN in Table 1).
- For the mainshock, the periods were those identified employing the examined seismic event (namely, E3 in Table 1) and the CSI input–output technique. The input was represented by the signals measured from the three-axial sensor at the base of the structure, while the output was the building response which was recorded by the sensors installed at the different storeys.

The reason for using these two different methods to estimate the building periods depending on the seismic input was that a noticeable variation of the frequencies identified was observed during different mainshocks and aftershocks across the entire set of observed seismic events, as one can see from Table 1 (adapted from Cattari et al. 2021); this even though the building responded in the pseudo-elastic field during the earthquake, as confirmed also by the nonlinear dynamic analyses performed on the numerical model.

As one can see from Fig. 6, the maximum frequencies for all the vibration modes were observed from the analysis of the ambient noise (AN in Fig. 6a and Table 1), even if this record was acquired after the most significant shakes of the earthquake swarm. Furthermore, the frequencies tend to decrease with increasing maximum  $PGA$  with an inverse linear correlation (Fig. 6b), despite no damage was detected on the structure. This frequency shift in buildings is a phenomenon that is known in literature (Clinton, 2006; Celebi, 2007; Ceravolo et al. 2017) even if not completely understood yet. It can be observed with or without structural damage and during strong earthquakes or weak forced vibrations (Spina

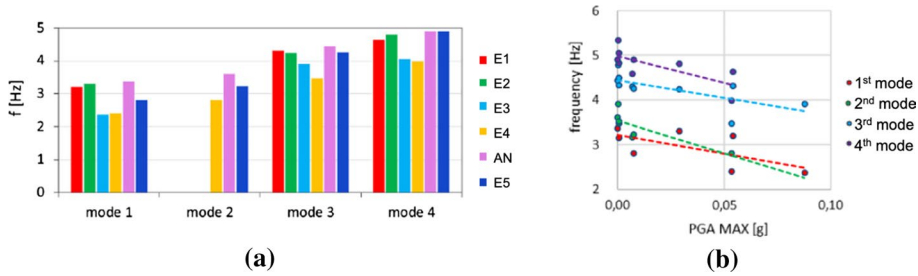


**Fig. 6** **a** Natural frequencies wandering of the first four modes obtained by data analysis from mainshocks and ambient vibrations. **b** Seismic wandering of the modal frequencies as a function of *PGA*. A linear fitting of data is assumed (figures adapted from Cattari et al. 2021)

and Lamonaca, 1998; Ceravolo et al. 2017), where it may be governed by the frequency characteristics of the input (Michel and Gueguen, 2010). In particular, it is an amplitude-dependent phenomenon, that can be composed of a transient (reversible) contribution and a permanent (irreversible) contribution. As already highlighted by Ceravolo et al. (2017) and Lorenzoni et al. (2013), the reversible phenomenon is mainly ascribable to various sources, e.g. reversible material and geometrical nonlinearities, soil-structure interaction, interaction between structural and nonstructural elements. However, if no structural damage occurs, the frequency shift gradually vanishes in time and the pre-seismic values of natural frequencies are completely recovered. Since this transient phenomenon cannot be properly caught by nonlinear static analyses, the Authors decided to use the periods experimentally identified by employing the examined seismic event for the mainshock of 26/10/2016, while the modal periods of the numerical model for the secondary event of 19/04/2014. However, how this difference would affect the results will be showed and discussed in Sect. 5.2 (Fig. 11).

Concerning the mode shapes and the modal participation coefficients, they were assessed from the calibrated EF model, assuming that the mode shapes had no significant variation during the mainshock of 26th October 2016. The latter assumption is licit, as the modal displacements at the nodes where sensors are installed were unchanged (Cattari et al. 2021).

In conclusion, Table 2 summarizes the values of periods and damping used for the floor spectra computation for each mode and seismic event. It has to be specified that the damping values were obtained employing the two-step procedure described at Sect. 4.1 for the

**Table 2** Periods and structural damping used for each mode in the floor spectra evaluation (step 2)

Event	Input data	Mode 1	Mode 2	Mode 3	Mode 4	Mode 5	Mode 6	Mode 7	Mode 8
19th April 2014	$T_k$ (s)	0.293	0.286	0.226	0.191	0.139	0.136	0.128	0.108
	$\xi_k$ (%)	5	4	5	5	5	5	5	5
26th October 2016	$T_k^*$ (s)	0.424	0.356	0.256	0.247	0.186	0.178	0.151	0.133
	$\xi_k$ (%)	4	5	10	5	5	5	5	5

\*Periods identified with the examined event (E3 in Table 1) using input–output analysis. Modes from 5 to 8 (not identified during the mainshock) are the one obtained from the analysis of the ambient noise (AN in Table 1) acquired after the earthquake swarm

all the modes which contributed the most to the floor spectra (*i.e.* modes 1 to 3, that are those with a significant contribution in terms of product  $P$ , as better clarified in the following section). On the contrary, a damping equal to 5% was assumed for all the others. As one can see from Table 2, the obtained values are around 5%, as expected in the elastic or pseudo-elastic response; a higher value was obtained only for mode 3 and for the mainshock of October. However, this result is in line with the experimental damping (see  $\xi_{exp}$  in Table 3, evaluated as the ratio between the peak and the  $PFA_{exp}$ ) and with the damping identified with input–output analysis (even if the latter are in general lower).

## 5.2 Floor spectra evaluation

Figure 7 shows the  $PFA/PGA$  profiles along the longitudinal direction and for the sensors placed along the same VA, as identified on the axonometry in Fig. 1a. The dashed plots refer to the values of  $PFA$  analytically obtained and compared with the experimental ones (continuous plots).

Some considerations can be drawn:

**Table 3** Damping evaluation for each sensor (step 1): secondary event of 19th April 2014 and mainshock of 26th October 2016 (values in brackets)

Dir X	Level	Sensor id	Dominant mode	Secondary mode	$\xi_{fit}$ (%)	$\xi_{exp}$ (%)	$PFA/PFA_{exp}$ (–)	
VA1	1	9	3	0	4.4 (7.9)	7.9 (12.2)	0.71 (0.77)	
	2	15	3	0	4.6 (9.7)	6.2 (9.6)	0.84 (1.01)	
	3	22	3	0	5.0 (11.4)	5.9 (8.9)	0.90 (1.17)	
	VA2	1	11	3	0	3.5 (7.1)	5.1 (9.9)	0.80 (0.83)
		2	17	3	0	4.2 (10.2)	4.2 (10.2)	1.00 (1.01)
		3	25	3	0	4.2 (11.2)	4.2 (10.2)	1.01 (1.06)
	VA4	1	13	3	0 (–4)	3.6 (4.4)	7.1 (10.1)	0.69 (0.64)
		2	20	3	0 (–4)	4.0 (6.1)	6.1 (9.1)	0.80 (0.83)
		3	27	3	0 (–4)	4.1 (6.7)	7.0 (10.0)	0.76 (0.83)
VA3	1	8	3	0	7.4 (14.0)	5.3 (10.4)	1.27 (1.28)	
	2	19	3	0	6.9 (18.2)	4.5 (10.5)	1.35 (1.50)	
	3	24	3	0	6.3 (17.6)	4.8 (10.6)	1.23 (1.45)	
Dir Y	Level	Sensor id	Dominant mode	Secondary mode	$\xi_{fit}$ (%)	$\xi_{exp}$ (%)	$PFA/PFA_{exp}$ (–)	
VA1	1	10	2	0	3.8 (4.68)	7.9 (6.6)	0.68 (0.83)	
	2	16	2	0	3.8 (5.4)	5.7 (5.8)	0.80 (0.97)	
	3	23	2	0	3.9 (5.9)	6.1 (6.0)	0.78 (1.01)	
VA2	1	12	1	2,8	3.0 (2.6)	12.7 (9.3)	0.55 (0.60)	
	2	18	1	2	4.2 (3.8)	11.5 (9.3)	0.65 (0.72)	
	3	26	1	2	4.1 (4.5)	11.1 (10.0)	0.68 (0.78)	
VA4	1	14	1	0 (–2)	5.5 (4.4)	9.1 (4.5)	0.79 (1.06)	
	2	21	1	0 (–2)	5.6 (4.8)	9.0 (4.4)	0.79 (1.11)	
	3	28	1	0 (–2)	5.7 (4.9)	11.4 (4.9)	0.70 (1.07)	



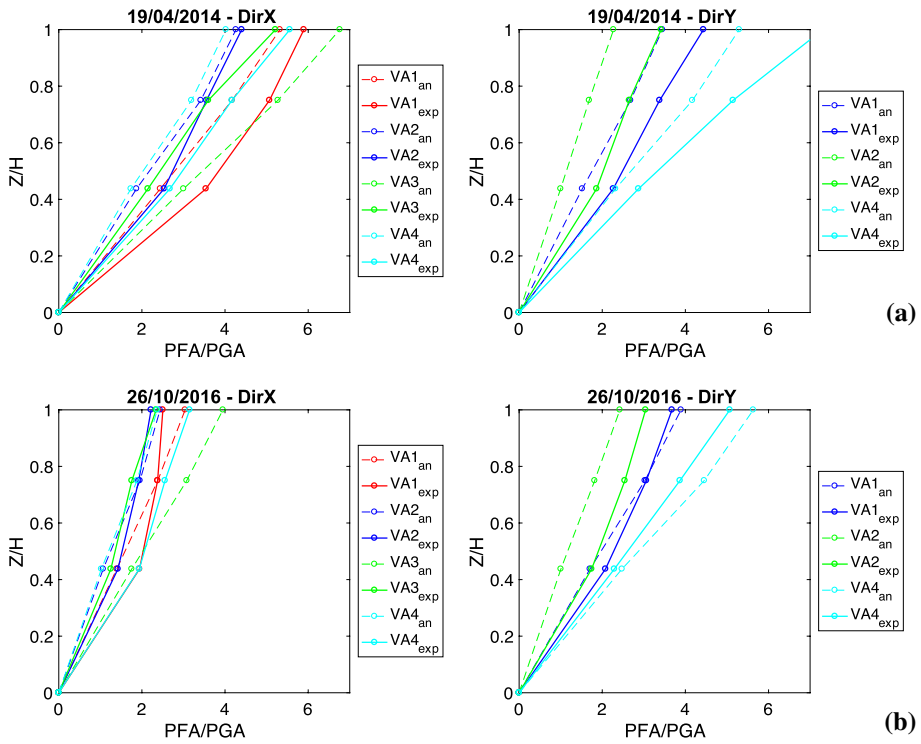


**Fig. 7** PFA/PGA profile along the height of the building: comparison between analytical (dashed plot) and experimental profiles (continuous plot) for the two examined seismic events: **a** minor event of 19/04/2014 and **b** mainshock of 26/10/2016

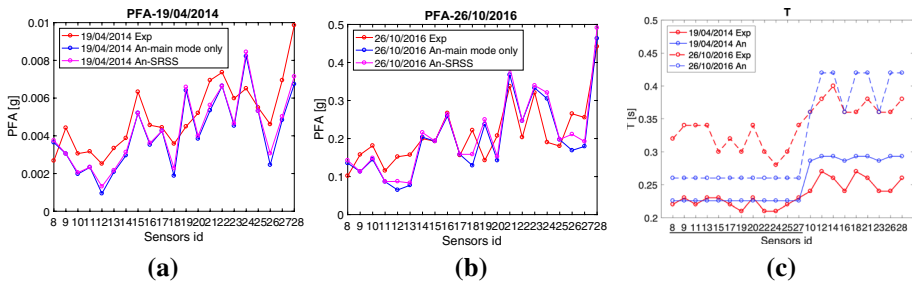
- The maximum value of *PFA/PGA* measured by the monitoring system is generally between 2 and 6 and it is registered at the top floors. The amplification is reduced in the X direction of the mainshock, while it is quite similar comparing the two events in the Y direction.
- Analytical profiles tend generally to underestimate the experimental ones. This is expected, since the *PFA* is affected by multimodal contribution more than the spectral peak. Furthermore, this underestimation could be due to the differences between numerical and experimental mode shapes highlighted by the MAC indexes (Fig. 3c).
- Despite the complexity of the building, the shape of the profiles is roughly linear for all the VAs, since the dynamic response of the structure is mainly dominated by the contribution of the fundamental modes in the two main directions (mode 3 in the X direction and modes 1 and 2 in the Y direction—see also Table 3). This is typical of low-rise building. Conversely, a significant influence of higher vibration modes is expected for high-rise buildings and this influence leads to a multilinear and non-monotonous shape of profiles, as for example numerically observed also by Di Domenico et al. (2021). However, for some sensors the multimodal contribution is more relevant, as better discussed in the following of this section.

Figure 8a,b illustrates the comparison between the experimental and analytical values of *PFA* for both the seismic events and for each sensor, while Fig. 8c reports the periods *T*. In particular, in Fig. 8a–b the analytical *PFA* are evaluated alternatively considering the contribution of the dominant mode only [*i.e.* the one characterized by the highest value of the product *P*—Eq. (6) in Sect. 4] or combining the contribution of the selected modes with a square root of sum of squares (SRSS) rule. The analytical plots of *PFA* are respectively colored in blue and magenta, while the experimental ones are in red. Instead, in Fig. 8c, the experimental periods (in red) are those evaluated in correspondence of the maximum recorded spectral acceleration peaks, while the analytical ones (in blue) are those which correspond to the modes with the highest contribution again in terms of *P*. It has to be recalled that the sensors underlined on the X-axis in Fig. 8c are the ones in the X direction. The sensors placed at the foundation level (from 1 to 7) are not reported, since not interesting within the aims of this paper.

From Fig. 8, it is possible to see that:

- The major contribution to the floor spectra is due to the fundamental mode in the direction of analysis for all the sensors except for the ones aligned along VA2y (sensors n. 12, 18 and 26): here, in fact, the dominant mode is mode 1, but the dynamic response is also affected by the contribution of mode 2, even if to a lesser degree ( $P_{norm}$  around 60%—see Table 3).
- The correspondence between analytical and experimental periods is quite good for both the events in the Y direction and for the minor event in the X direction, while the analytical periods underestimate the experimental ones in the X direction and for the mainshock.
- It is possible to observe a period elongation, due to the frequency shift already described in Sect. 5.1, passing from the minor to the main event.

Figure 9 shows instead the comparison between the recorded (continuous plot, labelled as “exp”) and analytical (dashed plot, labeled as “an”) acceleration floor spectra for the two events at the sensors located along the same VA. The comparison appears in general satisfying, even if the analytical floor spectra of some VAs don’t match well the experimental ones (*e.g.* VA3x and VA4x for the mainshock of 26/10/2016). This could be dependent on the major complexity of the dynamic behaviour of this case-study, as also demonstrated by the irregular shapes that characterize experimental floor spectra.



**Fig. 8** Comparison, for each sensor between: **a** analytical and experimental *PFA*—minor event of 19/04/2014, **b** analytical and experimental *PFA*—mainshock of 26/10/2016, **c** analytical and experimental periods *T* for both the events

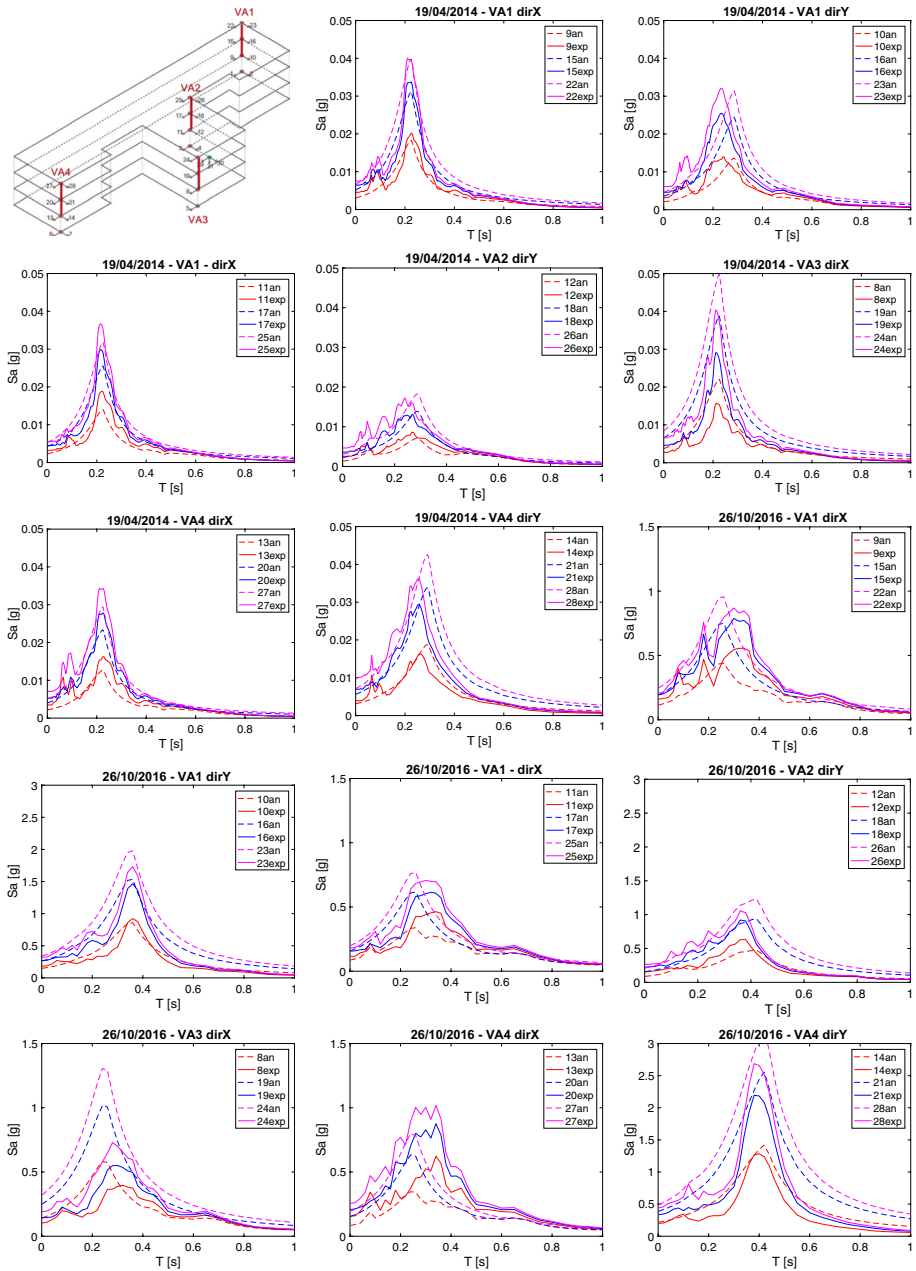


**Fig. 9** Floor spectra for the minor event of 19/04/2016 and the mainshock of 26/10/2016: comparison between experimental (continuous plot) and analytical ones (dashed plot)

One consequence of this complexity was a more difficult calibration of the numerical model with MAC indexes lower than the values obtained for the other case-study (even if more than satisfying). The results of the calibration (used as input for the validation) may have affected the comparison illustrated in Fig. 9.

Table 3 shows the damping factors obtained for each sensor from the experimental data (“step 1” of the procedure explained at Sect. 4.1). It has to be specified that the values of  $\xi_{fit}$ ,  $\xi_{exp}$  and  $PFA/PFA_{exp}$  presented in brackets refer to the mainshock of 26th October 2016, while the others to the minor event of 19th April 2014. In particular, the table collects, for each sensor and VA:

- The dominant mode.
- The secondary mode, that was the one characterized by a contribution in terms of  $P_{norm}$  respectively higher than 60% (if the number in the table is positive) or higher than 30% (if the number is negative).
- The fitted structural damping ( $\xi_{fit}$ ), obtained to guarantee for each sensor the best fitting between the analytical peak determined on the dominant mode and the experimental one.
- The experimental structural damping ( $\xi_{exp}$ ), obtained from the ratio between the experimental peak and the experimental  $PFA$ .
- The ratio between analytical and experimental  $PFA$ .

Concerning the ratio  $PFA/PFA_{exp}$ , it has to be pointed out that when this ratio is higher than one, it means that the numerical calibrated model (from which the values of  $\Gamma$  and  $\Phi$  were calculated) overestimates the experimental response. Thus, a higher damping factor is necessary to compensate for this overestimation. On the contrary, if the ratio is lower than 1, the experimental response is underestimated, and the fitted structural damping is lower. In other words, when the  $PFA/PFA_{exp}$  ratio is around 1, it means that the numerical model catches well the experimental response; as a consequence,  $\xi_{fit}$  is almost equal to  $\xi_{exp}$ . This would be completely rigorous if  $\xi_{exp}$  would be evaluated as the ratio between the peak and the contribution of the  $PFA$  due to that mode; otherwise, when the  $PFA$  is influenced by many modes, the obtained damping is overestimated, because the experimental ratio becomes lower than that one we would use to evaluate  $\xi_{exp}$ . Thus, when the floor spectrum is influenced by the contribution of many modes, the ratio  $PFA/PFA_{exp}$  is affected by the underestimation of  $\xi_{exp}$ , as well.

As one can see from the table, for the sensors placed in the X direction, the dominant mode is usually mode 3, while for the sensors in the Y direction, the dominant modes are mode 1 (for the sensors placed along VA2 and VA4) and mode 2 (for the sensors placed along VA1). Moreover, sometimes the response is also affected by higher modes, whose contribution can affect more (as for VA2y) or less (as for VA4x and VA4y) the final floor spectra. For example, this is evident from Fig. 10 for the sensor 12 where a not negligible contribution is due to modes 1 (the dominant mode) 2, 8 (secondary modes with  $P_{norm}$  higher than 60%) and 7 (secondary mode with  $P_{norm}$  lower than 30%).

It has to be pointed out that, from the analysis of the experimental data, it is quite clear that the structure filters also the frequency in correspondence of the peaks present in the seismic input. This is for example highlighted in the experimental floor spectrum of sensor 22 of Fig. 10 (black line), which has two peaks: one at the fundamental period and the other at a lower period with a not negligible frequency content present in the input. However, this aspect cannot be taken into consideration by the proposed

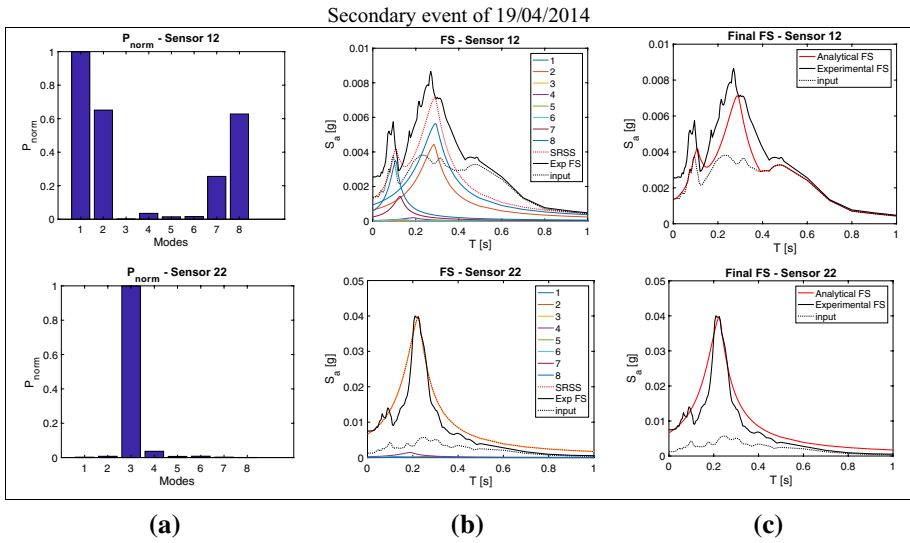


**Fig. 10** a Contribution of modes in terms of  $P_{norm}$ . b Floor spectra evaluated for each mode. c Final floor spectra computed with Eq. (1)

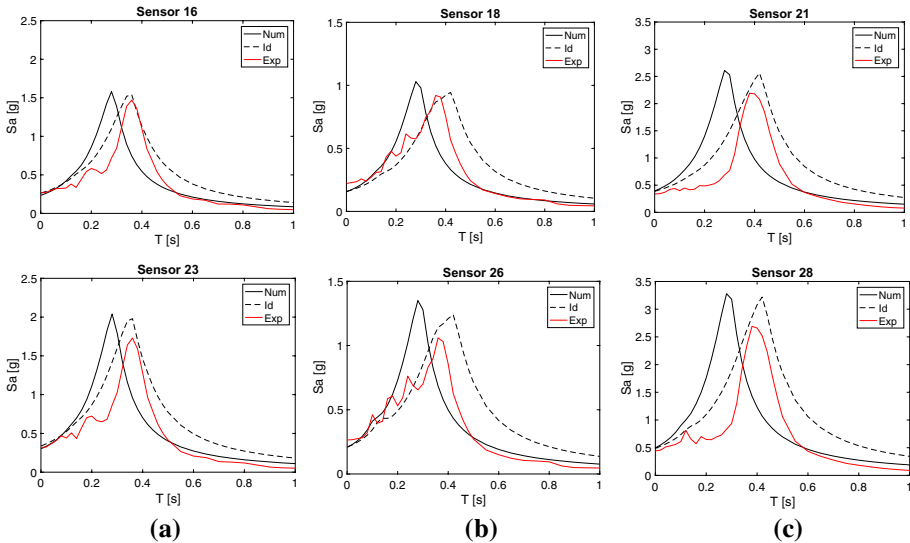


**Fig. 11** Comparison between experimental (labeled as “Exp” and plot in red) and analytical (in black) floor spectra for the mainshock of 26/10/2016. The latter were respectively obtained using: the numerical modal parameters (labeled as “Num” – continuous plot) and the ones identified with the examined event (labeled as “Id” – dashed plot): a VA1Y. b VA2Y. c VA4Y

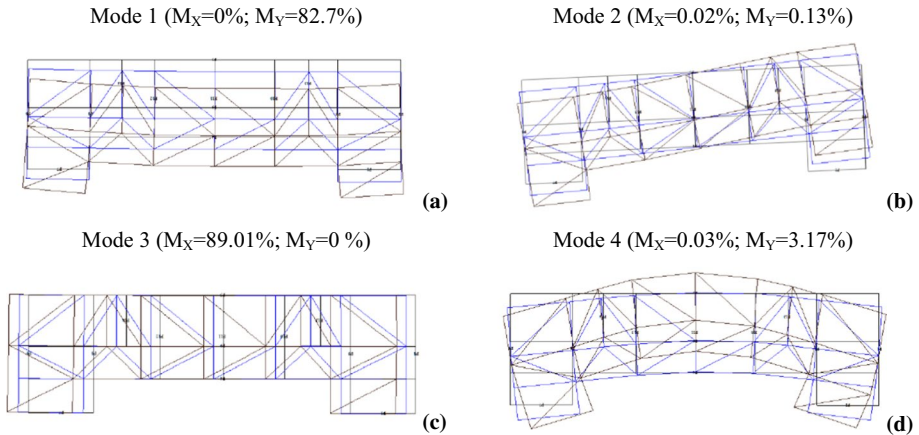


**Fig. 12** Numerical mode shapes of the Pizzoli's town hall: **a** mode 1, **b** mode 2, **c** mode 3, **d** mode 4

formulation, which instead considers the value of the ground response spectrum only at the fundamental periods of the building.

Finally, Fig. 11 shows the sensibility of the proposed expression to the choice of the natural periods of the selected modes. Since, as above-mentioned, no appreciable structural damage occurred on the courthouse, it could be considered reasonable using the modal parameters of the numerical model also for the floor spectra evaluation of the main-shock of October 2016. This would be the strategy followed by practitioners, who could not necessarily benefit from the results of the dynamic identification to estimate the structural parameters. The application of the analytical expression with the elastic modal periods obviously would not be able to properly describe the frequency shift observed for this case-study. In Fig. 11, the analytical floor spectra evaluated using the modal parameters computed from the numerical Tremuri model (labeled as “Num”—continuous plot) are compared with the ones identified with the examined event (labeled as “Id”—dashed plot). The latter are compared with the experimental ones obtained from the monitoring system (labeled as “Exp” and drawn in red). The comparison is shown for the three VAs with sensors in the Y direction (namely VA1, VA2 and VA4). From Fig. 11, it is possible to see that the floor spectra computed with the periods identified with the seismic event (dashed plot) fit better the experimental ones, which have a maximum amplification peak in correspondence of a period longer than the ones computed from the numerical modal analysis.

## 6 Application to the Pizzoli's town hall

### 6.1 Assessment of data used as input for the analytical computation of floor spectra

This section describes the application to the second case-study. In particular, the results will be presented following the same outline already illustrated for the former courthouse of Fabriano. In order to avoid repetitions, only the peculiar aspects and the main differences will be commented in the text.



As for the previous case-study, the ground response spectrum was computed from the accelerations recorded by the three-axial sensor placed at the building foundation (sensors n.15 and n.16 of Fig. 1b). In particular, the recordings of the secondary event of the 25th July 2015 (with  $PGA$  values around 0.001 g) and of the mainshock of 18th January 2017 ( $PGA_x=0.112$  g;  $PGA_y=0.100$  g) were used for the floor spectra evaluation.

Unlike the previous case-study, the dynamic behavior is dominated by the first translation mode in each direction (with participant mass higher than 80%, see Fig. 12). Despite that, in the floor spectra evaluation the contribution of the first four modes were considered in order to highlight the differences with the former courthouse of Fabriano.

Periods, modal shapes and participation coefficients of each mode were computed as follows:

- As far the periods concern, for the floor spectra evaluation of the secondary event, the periods were the ones obtained from the modal analysis performed on the calibrated numerical model. Instead, for the floor spectra evaluation of the mainshock, the analysis of the occurred damage (Fig. 2) and of the numerical dynamic response simulated during the seismic event (Degli Abbati et al. 2022) showed that the structural response was in the moderate nonlinear field. Thus, an elongation of the fundamental periods was assumed, coherently also with the experimental evidence (Sect. 3). In particular, the elongated periods were computed accounting for a degradation of stiffness properties of masonry. The values were calibrated considering as target the periods experimentally identified with input–output techniques by employing the examined recording (ReLUIS projects, Task 4.1 – Cattari et al. 2018). Since the evaluation of the elongated period could be an issue into practice, a simplified expression to calculate it has been proposed in Degli Abbati et al. (2018). According to this expression (Eq. 7), the elongated period  $T_k$  should be assumed as a mean value between the initial elastic period  $T_{ke}$  and a scant period corresponding to the displacement demand  $\sqrt{\mu} \cdot T_{ke}$ , for the considered seismic input, where  $\mu$  is the ductility demand on the equivalent single degree of freedom (SDOF) representing the building:

$$T_k = T_{ke} \frac{1 + \sqrt{\mu}}{2} \quad (7)$$

- Concerning the mode shapes and the participation coefficients, also in this case they were assumed from the calibrated EF model developed in Tremuri, by assuming no change produced by damage induced by the seismic shock of 18th January 2017. Again, it was verified that the modal displacements obtained for the various mainshocks remained almost unchanged, meaning that no significant variation of the corresponding mode shapes took place (Cattari et al. 2018; Lorenzoni et al. 2019).

Finally, the damping factor of the building  $\xi_k$  (associated to each mode) was evaluated following the two-step procedure already described in Sect. 4.1.

Figure 12 shows the mode shapes of the first four modes obtained from the numerical model.

In particular, it is possible to see from the figure that mode 1 is a translational mode in the Y direction, while mode 3 is a translational mode in the X direction.

Table 4 collects instead the values of periods assumed in the floor spectra computation and the damping used for each mode and for each seismic event. For those modes with a negligible contribution in terms of product  $P$ , a damping equal to 5% was

**Table 4** Periods and structural damping assumed for each mode in the floor spectra evaluation (step 2)

Event	Input data	Mode 1	Mode 2	Mode 3	Mode 4
25th July 2015	$T_k$ (s)	0.225	0.181	0.142	0.115
	$\xi_k$ (%)	3	5	5	5
18th January 2017	$T_k$ (s)	0.283	0.224	0.184	0.113
	$\xi_k$ (%)	6	5	7	5

assumed (this is the case of modes 2 and 4). As one can see, the values of damping in Table 4 are coherent with the expected variation in the response, being around 5% in the linear response and a bit higher (around 7%) during the slight nonlinear phase.

### 6.2 Floor spectra evaluation

Figure 13 shows the *PFA/PGA* profiles along the longitudinal direction and for the sensors placed along the same VA, as identified on the axonometry in Fig. 1b. Comparing these data with the ones obtained for the first case-study, it is interesting to notice that:

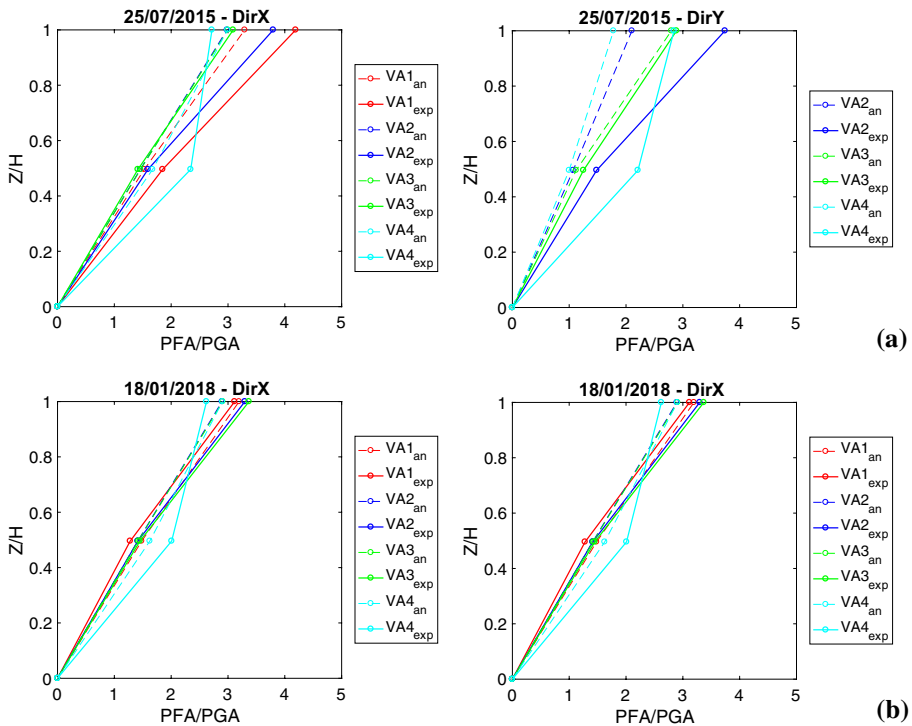
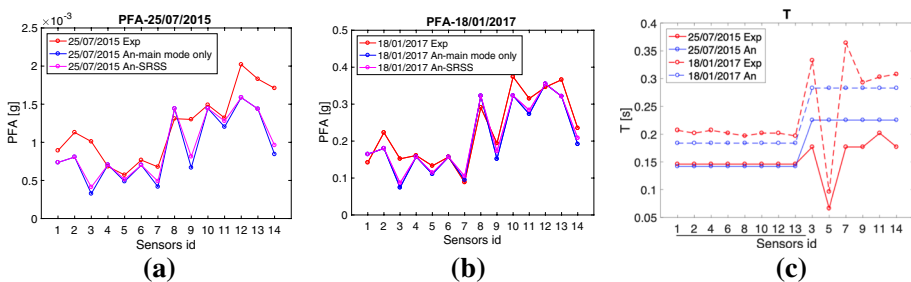


**Fig. 13** *PFA/PGA* profile along the height of the building: comparison between analytical (dashed plot) and experimental profiles (continuous plot) for the two examined seismic events: **a** minor event of 25/07/2015 and **b** mainshock of 18/01/2018

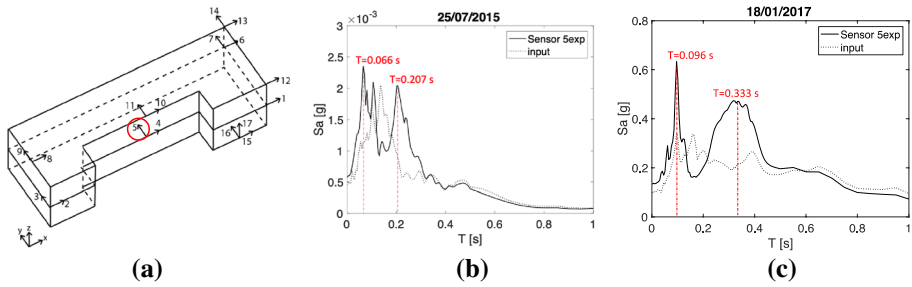
- Here the maximum value of  $PFA/PGA$  measured by the monitoring system is generally slightly lower (being between 2.5 and 4), but it is registered again at the top floors; observing the  $PFA/PGA$  profiles obtained from the recordings of 18/01/2018, it is possible to observe that this amplification is reduced, due to the damage induced by the earthquake on the structure.
- Analytical profiles tend to underestimate the experimental ones in both directions for the minor event of 25/07/2015, while they are able to catch the actual profiles in case of the mainshock of 18/01/2017.
- The profile shape differs depending on the considered VA: for most VAs, it is roughly linear, as expected for a regular 2-storey building with stiff diaphragms like the examined one, whose dynamic response is dominated by the contribution of the fundamental modes in the two main directions; however, it is interesting to observe that this almost linear shape becomes bi-linear for VA2 and VA4, probably due to the position of the sensors at the two edges of the plan and, consequently, to the influence of the torsional mode that here is maximum.

Figure 14 instead illustrates the comparison between experimental and analytical values of  $PFA$  for the two considered events and for each sensor (Fig. 14a,b). The periods  $T$  (Fig. 13c) are reported as well. As for the previous case-study, the sensors underlined on the X-axis in Fig. 13c are the ones in the X direction. From Fig. 13, it is possible to see that:

- The major contribution to the floor spectra is due to the fundamental mode in the direction of analysis (Fig. 14a,b). For this reason, the analytical  $PFA$  obtained computing only the main mode (blue plot) and the ones obtained considering the first four modes combined with the SRSS rule are almost identical.
- The correspondence between analytical and experimental periods is quite good, especially for the X direction. Moreover, a period elongation is observed passing from the minor event of 25/07/2017 (continuous plot) to the mainshock of 18/01/2017 (dashed plot) that is properly captured by the analytical expression (Fig. 14c). Only for sensor n.5 the experimental period is significantly lower than the ones detected in the other sensors and analytically evaluated as the period of the mode with the major contribution.



**Fig. 14** a Comparison, for each sensor, between: a analytical and experimental  $PFA$  – minor event of 25/07/2015, b analytical and experimental  $PFA$  – mainshock of 18/01/2017, c analytical and experimental periods  $T$  for both the events



**Fig. 15** **a** Sensor 5 location; Experimental floor spectra and identification of the maximum peaks: **b** minor event of 25/07/2015, **c** mainshock of 18/01/2018

In order to explain the mismatch on sensor n.5, looking at the results presented in Fig. 15b, it is possible to observe that in correspondence of this sensor the experimental floor spectrum has two spectral peaks: the first one around  $T=0.066$  s (this is the maximum spectral peak detected in Fig. 14c for the event of 25/07/2015); the second one (which is a bit lower) is instead approximately around the fundamental period in that direction, coherently with what obtained for the other sensors. The same shape characterizes the floor spectrum of the sensor obtained during the event of 18/01/2017 (see Fig. 15c). However, in this case, the two periods with the maximum values of amplification are:  $T=0.096$  s and  $T=0.3$  s; the latter is plausibly the fundamental period, elongated due to the structural non-linearity. Indeed, it is interesting to observe that a fifth mode with  $T=0.082$  s was experimentally identified by Sivori et al. (2021) and ascribed to the shear mode which activates the local response of diaphragms. Thus, it seems reasonable to conclude that, in the point where sensor n.5 is placed, the Pizzoli's town hall filters the ground motion in correspondence of two frequencies: the one which characterizes its global dynamic response and the one which characterizes the local response of diaphragms.

Figure 16 shows the comparison between the recorded (continuous plot, labelled “exp”) and analytical (dashed plot, labeled “an”) acceleration floor spectra for the two events computed for the sensors located along the same VA at the two levels. It should be pointed out that in the figure VA4 comprises sensors 2–3 at the first level and 8–9 at the second one, even not strictly aligned along the same vertical axis. The comparison shows a very good correspondence.

Finally, analogously with what already presented for the former courthouse of Fabriano, Table 5 reports the details of the analyses in terms of: dominant and secondary modes, damping factor for each sensor which guarantee the best fitting with experimental data ( $\xi_{fit}$ ), experimental structural damping ( $\xi_{exp}$ ) and ratio  $PFA/PFA_{exp}$ . Again, the values in brackets refer to the mainshock of 18th January 2017, while the values directly collected in the table refer to the secondary event of 25th July 2015. As one can see from the table, it is interesting to observe that: for the sensors placed in the X direction, only the dominant mode is relevant; for those placed in the Y direction, also the contribution of the secondary modes should be taken into account. This can be observed also from Fig. 17, which shows for two sensors placed at the second level of the building (sensor n.12 and n.9): (a) the importance of the selected modes in terms of  $P_{norm}$ ; (b) the floor spectra evaluated for each mode; (c) the final floor spectra, evaluated by the SRSS combination. As it is possible to see from Fig. 17, the floor spectra of sensor n.12 is characterized by only one peak (Fig. 17c) in correspondence of the period of mode 3

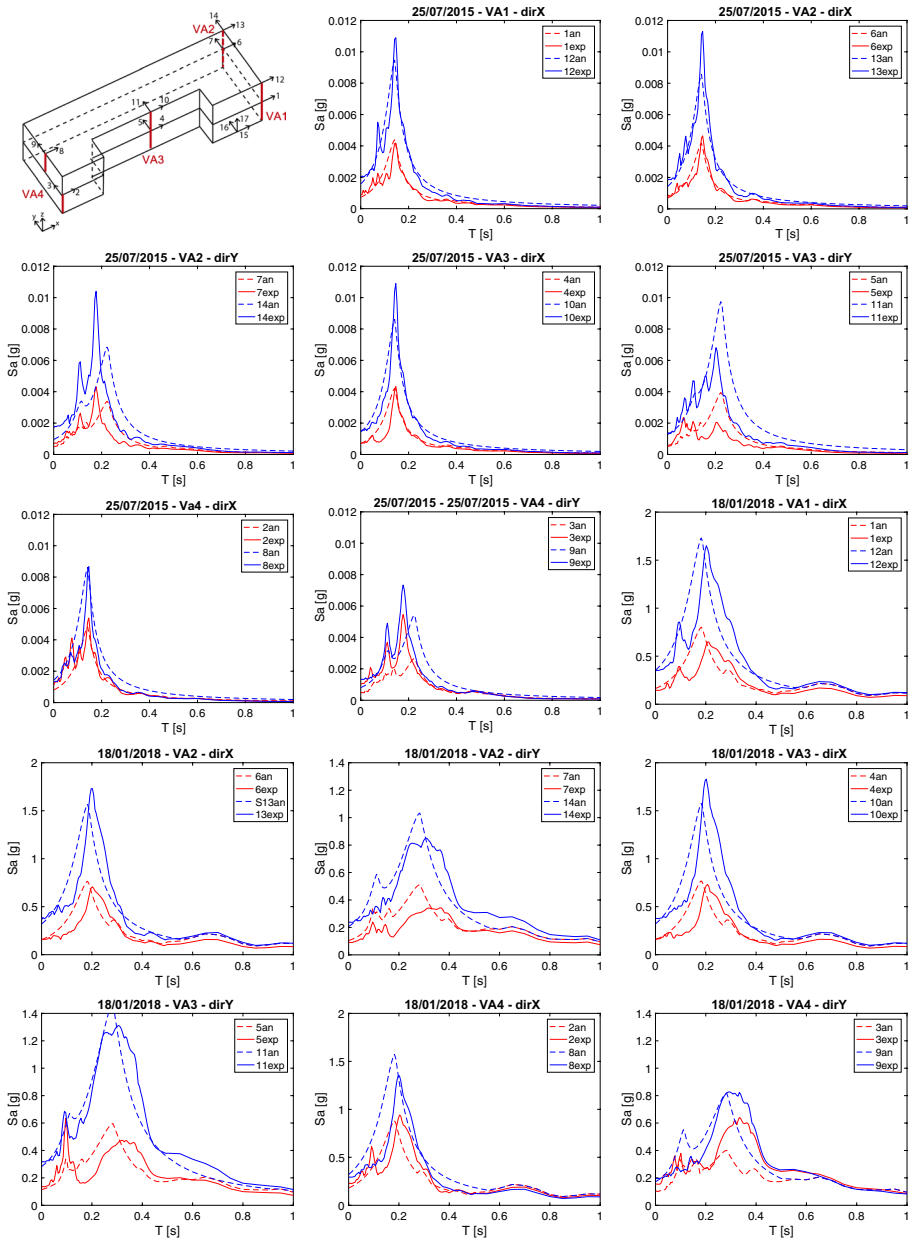


**Fig. 16** Floor spectra for the minor event of 25/07/2015 and the mainshock of 18/01/2017: comparison between experimental (continuous plot) and analytical ones (dashed plot)

(the fundamental one in the x direction); coherently, only the contribution of this mode is relevant (Fig. 17a), while the contribution of the others is negligible (Fig. 17b). On the contrary, the floor spectra of sensor n.9 show that two modes contribute the most:

**Table 5** Damping evaluation for each sensor (step 1): secondary event of 25th July 2015 and mainshock of 18th January 2017 (values in brackets)

Dir X	Level	Sensor id	Dominant mode	Secondary mode	$\xi_{\text{fit}}$ (%)	$\xi_{\text{exp}}$ (%)	PFA/PFA <sub>exp</sub> (–)
VA1	1	1	3	0	5.3 (9.0)	7.6 (8.0)	0.81 (1.08)
	2	12	3	0	4.2 (7.4)	6.0 (7.4)	0.82 (1.01)
VA2	1	6	3	0	4.4 (7.7)	5.0 (8.1)	0.94 (0.97)
	2	13	3	0	3.6 (6.3)	4.8 (7.5)	0.85 (0.90)
VA3	1	4	3	0	4.9 (7.4)	4.6 (8.0)	1.04 (0.96)
	2	10	3	0	3.8 (5.9)	3.6 (7.1)	1.03 (0.90)
VA4	1	2	3	0	4.4 (6.5)	7.4 (9.1)	0.74 (0.83)
	2	8	3	0	5.0 (8.4)	4.3 (7.7)	1.10 (1.05)
Dir Y	Level	Sensor id	Dominant mode	Secondary mode	$\xi_{\text{fit}}$ (%)	$\xi_{\text{exp}}$ (%)	PFA/PFA <sub>exp</sub> (–)
VA2	1	7	1	4	2.2 (9.0)	4.6 (10)	0.75 (1.07)
	2	14	1	4	1.8 (7.0)	4.9 (12)	0.60 (0.84)
VA3	1	5	1	–4	5.7 (6.0)	9.5 (7)	0.79 (0.87)
	2	11	1	–4	4.7 (7.0)	6.5 (9)	0.89 (0.87)
VA4	1	3	1	4	1.2 (3.0)	6.0 (9)	0.45 (0.63)
	2	9	1	4	2.0 (6.0)	5.6 (9)	0.65 (0.89)

modes 1 and 4 (Fig. 17a); in fact, the final floor spectra illustrated in Fig. 17c are characterized by two peaks, in correspondence of the periods associated with these two modes, whose contribution is computed in Fig. 17b.

## 7 Comparison with code proposals

This section presents the comparison with some code proposals, *i.e.* the one included in Sect. 4.3.5 of the Eurocode 8 and two of the three proposals included in Sect. 7.2.3 of the Commentary of the Italian Technical Code (2019) for nonstructural elements and local mechanisms. In fact, since the third expression included in the Commentary is specifically addressed only to buildings with a reinforced concrete frame structure, it is not considered for the aim of such a comparison.

Eurocode 8 proposes Eq. (8) to compute floor spectra whose theoretical derivation is however not clearly stated. This proposal will be defined as EC8 hereinafter. In Eq. (8),  $T$  is the fundamental period of the nonstructural element,  $T_1$  is the fundamental period of the building in the relevant direction,  $PGA$  is the peak ground acceleration,  $Z$  is the height of the nonstructural element above the level of application of the seismic action and  $H$  is the building height.

It is worth noting that if  $T=0$ , a linear  $PFA$  distribution along the building height is obtained varying the  $Z/H$  ratio. It can be noticed that  $PFA$  ranges from  $PGA$  (when  $Z=0$ ) to  $2.5PGA$  (when  $Z/H=1$ ), while the maximum  $S_{a,Z}(T)$  is always obtained when  $T=T_1$ . If  $T$  equals  $T_1$ , the maximum  $S_{a,Z}(T)$  ranges from  $2.5PGA$  (if  $Z=0$ ) to  $5.5PGA$  (if  $Z=H$ ). It is interesting to observe that this expression doesn't include the effect of damping features



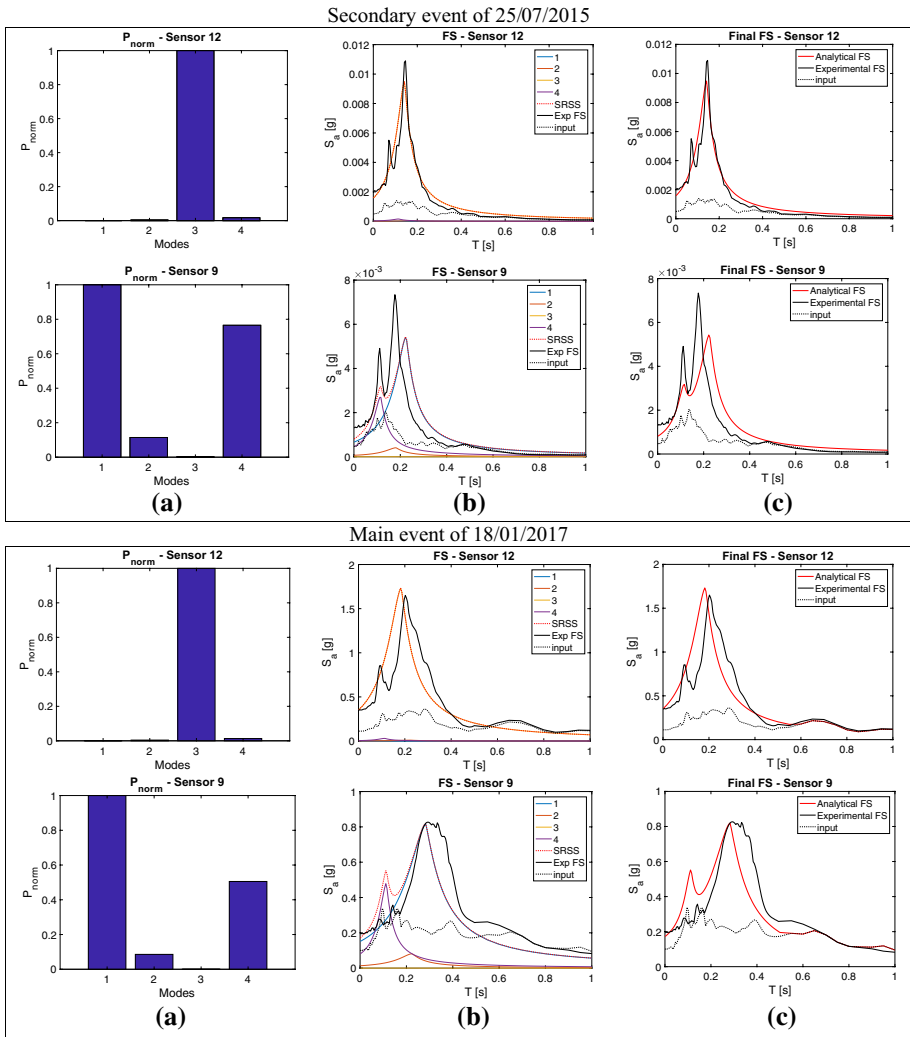


**Fig. 17** **a** Contribution of modes in terms of product  $P_{norm}$ . **b** Floor spectra evaluated for each mode. **c** Final floor spectra computed with Eq. (1)

(neither the damping of the nonstructural element, nor the one of the building); thus, it is impossible to quantify the effects of nonlinearity with this expression. Furthermore, it only allows considering the various position of the secondary element along the building height, while it makes impossible to take into account torsional effects or effects due to diaphragm flexibility associated to a different position of the element in plan.

$$S_{a,z}(T) = PGA \left[ \frac{3(1 + Z/H)}{1 + (1 - T/T_1)^2} - 0.5 \right] \geq PGA \tag{8}$$

The Commentary of the Italian Technical Code proposes two different expressions to compute floor spectra: both are addressed to the seismic assessment of nonstructural elements or local mechanisms, but the first one refers to a “rigorous” approach, while the second one is a “simplified” analytical formulation. Both account for multimodal contributions and for the effect of structural nonlinearity on floor spectra.

The “rigorous” method (defined as NTC1 hereinafter) accounts for multimodal contributions based on simple considerations related to structural dynamics. In fact, Eq. (9) gives the contribution of the  $k$ th vibration mode to the acceleration floor spectra at the  $Z$ th floor of the building as:

$$S_{aZ,k}(T, \xi) = PFA_{Z,k} \cdot R\left(\frac{T}{T_k}; \xi\right) \quad (9)$$

where  $PFA_{Z,k}$  is the contribution to the  $PFA$  given by the  $k$ th mode at the  $Z$ th building floor, while  $R$  is an amplification (or de-amplification) factor of the  $PFA$  which depends on the natural periods of the main structure ( $T_k$ ) and on the period and damping feature of the nonstructural element ( $T$  and  $\xi$ , respectively).

$PFA_{Z,k}$  is calculated as:

$$PFA_{Z,k} = \Gamma_k \Phi_{Z,k} S_a(T_k) \quad (10)$$

where  $\Gamma_k$  is the modal participation factor for the  $k$ th vibration mode,  $\Phi_k$  is the modal displacement of the  $Z$ th storey for  $k$ th vibration mode,  $S_a(T_k)$  is the spectral acceleration of the structure associated with its  $k$ th vibration period.

$R$  is instead calculated as:

$$R = \left[ \left( 2\xi \frac{T}{T_k} \right)^2 + \left( 1 - \frac{T}{T_k} \right)^2 \right]^{-\beta} \quad (11)$$

where  $\beta$  is a coefficient (ranging from 0.4 and 0.5) which takes into account the coupling between each building structural mode and the vibration mode of the secondary element. If  $T = T_k$ ,  $R = 1/(2\xi)$  according to Eq. (11) and the maximum value of  $S_{aZ,k}$  becomes  $1/(2\xi)$  times  $PFA_{Z,k}$  [Eq. (9)]. The result of the maximum amplification is a classical result of the dynamic of the damped SDOF system, even if obtained with a slightly different and less rigorous formulation. For each storey, the floor spectrum is finally obtained as a combination of multimodal contributions through the SRSS rule. Thus, it has a spectral shape with multiple peaks corresponding to the number of significant modes considered.

The Commentary of the Italian Technical Code suggests also a “simplified” analytical formulation for nonstructural elements and local mechanisms. This formulation (defined as NTC2 hereinafter) allows computing the acceleration floor spectrum  $S_{aZ}(T, \xi)$  at the level  $Z$  where the element is placed as the SRSS combination rule of the contribution provided by all the relevant modes considered [Eq. (12)]. The expression is based on the dynamic properties of the main structure (natural periods  $T_k$ , modal participation factor  $\Gamma_k$  and modal displacement  $\Phi_k$  for the  $k$ th vibration mode) and on the value of the seismic response spectrum at the base of the building in correspondence of the natural periods  $S_a(T_k)$ . Moreover, it depends on the damping feature of the main structure ( $\xi_k$ , related to the  $k$ th mode) and on the one of the nonstructural element, introduced through the damping correction factor  $\eta(\xi)$  computed by Eq. (5).

$$S_{aZ}(T, \xi, Z) = \sqrt{\sum (S_{aZ,k}(T, \xi))^2} (\geq S_a(T, \xi) \text{ for } T > T_1) \tag{12}$$

Equations (13) and (14) give the contribution provided by the  $k$ th mode of the main structure, respectively to the floor spectrum and the PFA.

$$S_{aZ,k}(T, \xi, Z) = \begin{cases} \frac{1.1 \xi_k^{-0.5} \eta(\xi) PFA_{Z,k}(Z)}{1 + [1.1 \xi_k^{-0.5} \eta(\xi) - 1] \left(1 - \frac{T}{aT_k}\right)^{1.6}} & \text{for } T < aT_k \\ 1.1 \xi_k^{-0.5} \eta(\xi) PFA_{Z,k}(Z) & \text{for } aT_k \leq T < bT_k \\ \frac{1.1 \xi_k^{-0.5} \eta(\xi) PFA_{Z,k}(Z)}{1 + [1.1 \xi_k^{-0.5} \eta(\xi) - 1] \left(\frac{T}{bT_k} - 1\right)^{1.2}} & \text{for } T \geq bT_k \end{cases} \tag{13}$$

$$PFA_{Z,k}(Z) = S_a(T_k, \xi_k) |\Gamma_k \Phi_k(Z)| \sqrt{1 + 4\xi_k^2} \tag{14}$$

The two coefficients  $a$  and  $b$  in Eq. (13) define the range of maximum amplification of the floor spectrum; they can be assumed respectively equal to 0.8 and 1.1. They are introduced in order to define a plateau of maximum amplification and overcome in this way the uncertainties related to the identification of the structure natural periods. Finally, the expression allows considering the decrease of amplification due to nonlinearity by means of an equivalent viscous damping  $\xi_k$  and an elongated equivalent period  $T_k$ .

Figure 18 compares the floor spectra computed applying the above-mentioned code proposals for some sensors (identified in Fig. 1) of the two examined case-studies. The latter are compared with the experimental ones (in black and labelled “exp” in Fig. 18) and with

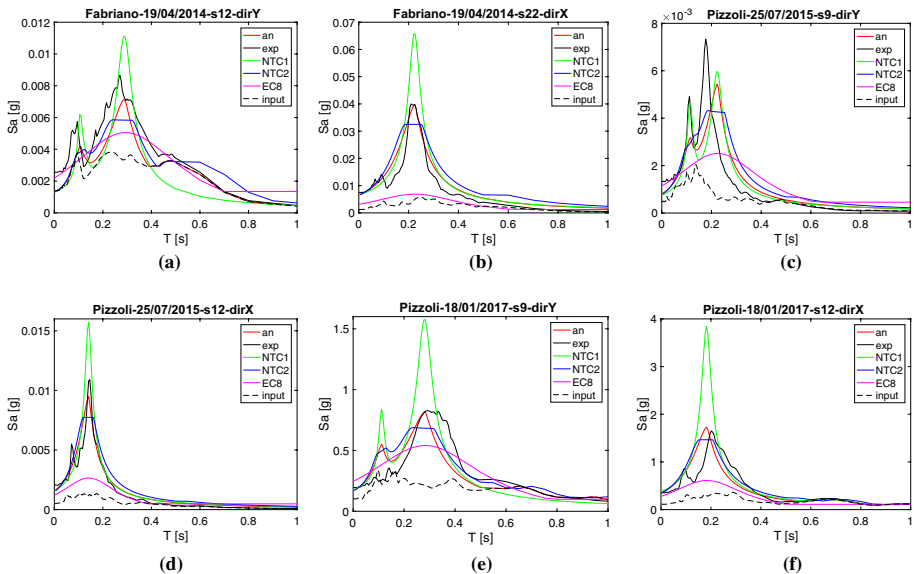


**Fig. 18** Comparison among code proposals: minor event of 19/04/2014 for the Fabriano courthouse, sensor n.12 **a** and n.22 **b**; minor event of 25/07/2015 for the Pizzoli’s town hall, sensor n.9 **c** and n.12 **d**; main event of 18/01/2017 for the Pizzoli’s town hall, sensor n.9 **e** and n.12 **f**

the ones evaluated applying the literature proposal by Degli Abbatì et al. (2018) presented in Sect. 4 (in red and labelled “an” in Fig. 18).

The same data employed in the previous sections for the validation (in terms of buildings dynamic properties and damping features) are here used to apply the code proposals in order to guarantee a consistent comparison. The seismic response spectrum at the base computed in correspondence of the buildings natural periods ( $S_a(T_k)$ ), necessary to apply the expressions prescribed in the Commentary of the Italian Technical Code, were computed as the integral in a proper range of periods around  $T_k$ , assumed equal to  $T_k \pm 0.06$  s, consistently with the criteria illustrated in Sect. 4.1. This expedient reduced the sensitivity to the irregular shape that characterizes seismic response spectra from actual records. Moreover, in the EC8 proposal,  $Z/H$  is assumed alternatively equal to 1 for the sensors placed at the top of the buildings (n. 22 for the Fabriano courthouse and n. 9 and n. 12 for the Pizzoli’s town hall) or equal to 0.42, for sensor n. 12 that is placed at the top of the first floor in the Fabriano’s courthouse. Finally, in the NTC1 proposal (“rigorous” method – Eqs. (9), (10), (11)), the  $\beta$  coefficient was assumed equal to 0.5; this is coherent with the hypothesis to assume the decoupling between main building and nonstructural element, that was assumed in the validation phase presented in the previous sections.

The sensors presented in Fig. 18 were selected in order to test the reliability of the code proposals to properly describe the effects of the various position in plan and height of the possible nonstructural elements (see the sensor layout in Fig. 1 for the two case-studies), the effects of multimodal contributions, the effects of nonlinearity (by comparing the floor spectra of the events of 25/07/2015 and of 18/01/2017 for the Pizzoli’s town hall).

From the comparison presented in Fig. 18, it is possible to observe that:

- Both NTC1 and NTC2 proposals catch quite well the amplification peak in the elastic phase, even if NTC1 tends sometimes to overestimate it and NTC2 tends to slightly underestimate it. Instead, the analytical expression proposed by the Authors (“an” in Fig. 18) stands between the two, with amplification peaks which are usually closer to the ones provided by NTC2. Furthermore, the NTC2 proposal overcomes the floor spectra sensitivity to the uncertainties in the identification of natural periods by defining a plateau of maximum amplification, while the NTC1 and the “an” proposal give floor spectra with sharper peaks. Thus, if the assumed period doesn’t perfectly match the period of experimental spectral amplification (e.g. in Fig. 18c), only NTC2 proposal compensates for this issue.
- The EC8 proposal is very simplified, thus it cannot be able to describe the structural nonlinearity as well as the contribution of higher modes and the effects due to a different position in plan of the possible nonstructural element. It only allows considering a different position along the building height (though the  $Z/H$  ratio), even if it seems to underestimate the amplification both in the elastic and in the nonlinear fields, at least for the two examined case-studies.
- Only NTC2 and the “an” proposal can catch the effects of structure nonlinearity, that are described by assuming an equivalent viscous damping and an elongated period for the building. In fact, the NTC1 proposal can only account for the nonlinearity of the nonstructural element  $\xi$  (that in this case was assumed always equal to 5%), while the EC8 proposal is independent on damping features of both the building and the nonstructural element.

- Both the proposals by the Commentary of the Italian Technical Code and the analytical proposal by the Authors can catch the multimodal contributions, that one can see from the experimental floor spectra of some sensors (*e.g.* sensor n. 12 in Fig. 18a, or sensor n. 9 Fig. 18c and e). On the contrary, the EC8 proposal can only consider the contribution of the fundamental vibration mode in the relevant direction.

## 8 Conclusions

Floor spectra are the tools currently prescribed by codes to evaluate the seismic demand on acceleration-sensitive nonstructural elements and local mechanisms in masonry buildings. For this reason, the validation of expressions available for their definition can significantly affect the results of seismic assessment procedures and, more generally, the engineering practice.

In this framework, this paper aims to validate a practice-oriented formulation proposed by the Authors in 2018, at the time only validated on the basis of some shake-table tests results, through the data acquired on two existing URM buildings hit by the last Central Italy earthquake. The two case-studies were selected because interesting for several reasons:

- The buildings were characterized by geometrical configurations of different complexity, allowing to investigate also the effects of higher modes contribution on the seismic response.
- Dynamic identification data were available for a detailed calibration of numerical models. The numerical models were then used to accurately interpret the dynamic response of these structures through nonlinear dynamic analyses.
- Recordings from different mainshocks and minor events were available from the permanent monitoring system and allowed an accurate comparison between measured and analytical floor spectra for the aim of validation of the practice-oriented approach proposed by the Authors.
- The two case-studies exhibited a different damage level after the 2016/2017 Central Italy earthquake, allowing to verify the reliability of the analytical approach both in the linear and moderated nonlinear fields.

The expected influence of some parameters on floor spectra (*e.g.* contribution of higher vibration modes, nonlinearity, torsional effects) has been confirmed by the monitoring data acquired by the OSS on the two buildings presented in the paper and by comparing these outcomes with the prediction of the literature formulation proposed by the Authors and the main code prescriptions. It has been observed that, among the available approaches proposed by codes, the two proposals included in the Commentary of the Italian Technical Code revealed quite appropriate for the assessment of floor spectra and easy to be implemented, being based on data achievable in the engineering practice with the effort compatible with that of common safety assessments; conversely, the methodology of Eurocode 8 seems too simplified, being unable to describe the structural nonlinearity as well as the contribution of higher modes and the effects due to a different position in plan of the possible nonstructural element. Finally, the expression proposed by the Authors turned out to be adequate to properly describe the amplification phenomenon, the multimodal contribution and the effects of nonlinearity. Furthermore, its explicit dependence on the mode shapes

allows implicitly to account for other aspects, such as the effects of diaphragm flexibility or torsion. As a result, the analytical expression can properly compute the floor spectra varying the position of the possible nonstructural elements in plan and in elevation. The approach is easy-to-use, because it requires only the basic structural dynamic properties and the expected seismic input, with an effort comparable to that of the Commentary of the Italian Technical Code. Results have proven that, provided a reliable estimate of dynamic properties, the analytical expression leads to a satisfactory matching with experimental floor spectra both in the linear and moderately nonlinear field. The need of the reliable estimate of dynamic properties highlights the usefulness of the monitoring or ambient vibration tests and that of efficient numerical models.

The recorded data from the two investigated structures showed that the building may amplify the input also in correspondence of those periods characterized by a not negligible spectral content. This aspect is not included in the proposed formulation that only considers the value of the spectral input at the base in correspondence of the natural period of the structure or at least in a small range around it. That could be improved in the future. Moreover, two further area of investigations are identified: the deepening of the frequency shift phenomenon, to provide also some easy-to-use approach to estimate it by engineers; a robust validation of the analytical expression also in a strong nonlinear field, possibly supported by nonlinear dynamic analyses carried out on calibrated models (since in this case accurate data on real structures able to document the phenomenon are very rare).

**Acknowledgements** The results presented in this paper have been obtained within the Italian national research project ReLUIS 2019–2021 (Work Package 6, Coord. Proff M.Savoia and F.Ponzo and Work Package 10, Coord. Prof. G.Magenes) founded by the Italian Civil Protection Agency. Moreover, the results presented in the paper benefited of the data made available by the Italian structural seismic monitoring network (OSS) of the Italian Department of Civil Protection, within the research activities of ReLUIS Project 2017–2018 (WP4 Task 4.1). The authors wish to acknowledge Eng. Daniele Spina for making the OSS data available.

**Authors' contributions** SDA: Methodology, Formal analysis, Data curation, Visualization, Writing – original draft; SC and SL: Supervision, funding, writing – review and editing. All authors read and approved the final manuscript.

**Funding** Open access funding provided by Università degli Studi di Genova within the CRUI-CARE Agreement.

## Declarations

**Conflict of interest** The authors declare that they have no conflict of interest.

**Open Access** This article is licensed under a Creative Commons Attribution 4.0 International License, which permits use, sharing, adaptation, distribution and reproduction in any medium or format, as long as you give appropriate credit to the original author(s) and the source, provide a link to the Creative Commons licence, and indicate if changes were made. The images or other third party material in this article are included in the article's Creative Commons licence, unless indicated otherwise in a credit line to the material. If material is not included in the article's Creative Commons licence and your intended use is not permitted by statutory regulation or exceeds the permitted use, you will need to obtain permission directly from the copyright holder. To view a copy of this licence, visit <http://creativecommons.org/licenses/by/4.0/>.



## References

- Allemange RJ and Brown DL (1982) A correlation coefficient for modal vector analysis, In: *Proceedings 1<sup>st</sup> international modal analysis conference*. November 8–10 1982, Orlando, Florida, pp 110–116
- Anajafi H, Medina RA (2019) Lessons learned from evaluating the responses of instrumented buildings in the United States: the effects of supporting building characteristics on floor response spectra. *Earthq Spectra* 35(1):159–191
- Anajafi H, Medina RA, Santini-Bell E (2019) Inelastic floor spectra for designing anchored acceleration-sensitive nonstructural components. *Bull Earthq Eng*. <https://doi.org/10.1007/s10518-019-00760-8>
- ASCE/SEI 7-10 (2010) Minimum Design Loads for Buildings and Other Structures. ASCE 7-10. Reston, VA: ASCE
- Baggio S, Berto L, Rocca I, Saetta A (2018) Vulnerability assessment and seismic mitigation intervention for artistic assets: from theory to practice. *Eng Struct* 167:272–286
- Beyer K, Tondelli M, Petry S, Peloso S (2015) Dynamic testing of a four-storey building with reinforced concrete and unreinforced masonry walls: prediction, test results and data set. *Bull Earthq Eng* 13(10):3015–3060
- Bothara JK, Dhakal RP, Mander JB (2010) Seismic performance of an unreinforced masonry building: an experimental investigation. *Earthq Eng Struct Dyn* 39:45–68
- Calvi PM, Sullivan TJ (2014) Estimating floor spectra in multiple degree of freedom systems. *Earthq Struct* 7(1):17–38
- Cattari S, Magenes G (2022) Benchmarking the software packages to model and assess the seismic response of unreinforced masonry existing buildings through nonlinear static analyses. *Bull Earthq Eng* 20(4):1901–1936. <https://doi.org/10.1007/s10518-021-01078-0>
- Cattari S, Degli Abbati S, Ottonelli D, Sivori D, Spacone E, Camata G, Marano C, Modena C, da Porto F, Lorenzoni F, Calabria A, Magenes G, Penna A, Graziotti F, Ceravolo R, Matta E, Miraglia G, Spina D, Fiorini N (2018) Report di sintesi sulle attività svolte sugli edifici in muratura monitorati dall'Osservatorio Sismico delle Strutture, Linea Strutture in Muratura, ReLUIS report (Task 4.1 Workgroup), Rete dei Laboratori Universitari di Ingegneria Sismica. *Technical Report* (in Italian)
- Cattari S, Degli Abbati S, Ottonelli D, Marano C, Camata G, Spacone E, da Porto F, Modena C, Lorenzoni F, Magenes G, Penna A, Graziotti F, Ceravolo R, Miraglia G, Lenticchia E, Fiorini N, Spina D (2019) Discussion on data recorded by the Italian Structural seismic monitoring network on three masonry structures hit by the 2016–2017 Central Italy Earthquake. *7th ECCOMAS Thematic Conference on Computational Methods in Structural Dynamics and Earthquake Engineering*, Crete, Greece
- Cattari S, Degli Abbati S, Alfano S, Brunelli A, Lorenzoni F, da Porto F (2021) Dynamic calibration and seismic validation of numerical models of URM buildings through permanent monitoring data. *Earthq Eng Struct Dyn* 50:2690–2711. <https://doi.org/10.1002/eqe.3467>
- Chen Y, Soong TT (1988) State of art review seismic response of secondary systems. *Eng Struct* 10:218–228
- Celebi M (2007) On the variation of fundamental frequency (period) of an undamaged building—a continuing discussion. *Proceedings of the Conference on Experimental Vibration Analysis for Civil Engineering Structures* October 24–26, Porto, Portugal. pp 317–326
- Ceravolo R, Matta E, Quattrone A, Zanotti FL (2017) Amplitude dependence of equivalent modal parameters in monitored buildings during earthquake swarms. *Earthq Eng Struct Dyn* 46:2399–2417
- Commentary of the Italian Technical Code (2019) Circolare esplicativa delle Norme Tecniche per le Costruzioni. Supplemento ordinario n. 5 Gazzetta Ufficiale 11 febbraio, 2019. (in Italian)
- Clinton J (2006) The observed wander of the natural frequencies in a structure. *Seismol Soc Am Bull* 96(1):237–257
- CESMD [Center for Engineering Strong-Motion Data] (2019) Accessed May 8, 2019. <https://strongmotioncenter.org/>
- Degli Abbati S, Cattari S, Lagomarsino S (2017) Proposta di spettri di piano per la verifica di elementi non strutturali e meccanismi locali negli edifici in muratura. *Proceedings ANIDIS - L'Ingegneria Sismica in Italia*, September 17–21–2017, Pistoia, Italy (in Italian)
- Degli Abbati S, Cattari S, Lagomarsino S (2018) Theoretically-based and practice-oriented formulations for the floor spectra evaluation. *Earthq Struct* 15(5):565–581. <https://doi.org/10.12989/eas.2018.15.5.565>
- Degli Abbati S, Cattari S, Lagomarsino S, Ottonelli D (2021) Seismic assessment and strengthening interventions of atop single-block rocking elements in monumental buildings: the case study of the San Felice sul Panaro Fortress. *SAHC 2020 - 12th International Conference on Structural Analysis of Historical Constructions*, Barcelona (Spain), 29–30 September–1 October 2021
- Degli Abbati S, Morandi P, Cattari S, Spacone E (2022) On the reliability of the equivalent frame models: the case study of the permanently monitored Pizzoli's town hall. *Bull Earthq Eng* 20(4):2187–2217. <https://doi.org/10.1007/s10518-021-01145-6>

- Derakhshan H, Nakamura Y, Griffith MC, Ingham JM (2020) Suitability of height amplification factors for seismic assessment of existing unreinforced masonry components. *J Earthq Eng*. <https://doi.org/10.1080/13632469.2020.1716889>
- Di Domenico M, Ricci P, Verderame GM (2021) Floor spectra for bare and infilled reinforced concrete frames designed according to Eurocodes. *Earthq Eng Struct Dyn*. <https://doi.org/10.1002/eqe.3523>
- Dolce M, Nicoletti M, De Sortis A, Marchesini S, Spina D, Talanas F (2017) Osservatorio sismico delle strutture: the Italian structural seismic monitoring network. *Bull Earthq Eng* 15(2):621–641
- Eurocode 8. Design of Structures for Earthquake Resistance. Part 1-1: General Rules, Seismic Actions and Rules for Buildings. Brussels; 2004:229
- Grünthal G. (ed.), Musson RMW, Schwarz J, Stucchi M (1998) European Macroseismic Scale. Cahiers du Centre Européen de Géodynamique et de Séismologie, Vol. 15 - European Macroseismic Scale 1998. European Center for Geodynamics and Seismology, Luxembourg
- Kazantzi AK, Vamvatsikos D, Miranda E (2020a) Evaluation of seismic acceleration demands on building nonstructural elements. *J Struct Eng* 146(7):04020118
- Kazantzi AK, Vamvatsikos D, Miranda E (2020b) The effect of damping on floor spectral accelerations as inferred from instrumented buildings. *Bull Earthq Eng* 18:2149–2164
- Lagomarsino S, Penna A, Galasco A, Cattari S (2013) TREMURI program: an equivalent frame model for the nonlinear seismic analysis of masonry buildings. *Eng Struct* 56:1787–1799
- Lorenzoni F, Casarin F, Modena C, Caldon M, Islami K, da Porto F (2013) Structural health monitoring of the Roman Arena of Verona Italy. *J Civil Struct Health Monit* 3(4):227–246
- Lorenzoni F, Lazzarini L, Calabria A, de Conto N, da Porto F (2019) Assessment of the dynamic response of monitored masonry buildings after the Central Italy earthquake swarm in 2016. *7th ECCOMAS Thematic Conference on Computational Methods in Structural Dynamics and Earthquake Engineering*, Crete, Greece
- Lucchini A, Franchin P, Mollaioli F (2017) Uniform hazard floor acceleration spectra for linear structures. *Earthq Eng Struct Dyn* 46(7):1121–1140
- Magenes G, Penna A, Senaldi IE, Rota M, Galasco A (2014) Shaking table test of a strengthened full-scale stone masonry building with flexible diaphragms. *Int J Archit Heritage* 8(3):349–375
- Martakis P, Reuland Y, Chatzi E (2022) Amplitude Dependency Effects in the Structural Identification of Historic Masonry Buildings. In: Pellegrino C, Faleschini F, Zanini MA, Matos JC, Casas JR, Strauss A (eds) Proceedings of the 1st conference of the european association on quality control of bridges and structures. EUROSTRUCT 2021. Lecture Notes in Civil Engineering, vol 200. Springer, Cham. [https://doi.org/10.1007/978-3-030-91877-4\\_17](https://doi.org/10.1007/978-3-030-91877-4_17)
- Menon A, Magenes G (2011a) Definition of seismic input for out of plane response of masonry walls: I. Parametric Study. *J Earthq Eng* 15(2):165–194
- Menon A, Magenes G (2011b) Definition of seismic input for out of plane response of masonry walls: II. Formulation. *J Earthq Eng* 15(2):195–213
- Merino RJ, Perrone D, Filiatrault A (2019) Consistent floor response spectra for performance-based seismic design of non-structural elements. *Earthq Eng Struct Dyn* 49(3):261–284
- Michel C, Guéguen P (2010) Time-frequency analysis of small frequency variations in civil engineering structures under weak and strong motions using a reassignment method. *Struct Health Monit* 9(2):159–171
- Muscolino G (1991). Dinamica di sistemi strutturali composti da due sottostrutture, Chapter contribution to the book “Problemi Strutturali nell’Ingegneria Sismica”, Dario Flaccovio Editore, pp 255–302 (in Italian)
- NZSEE (2017) New Zealand Society for Earthquake Engineering (NZSEE), Structural Engineering Society New Zealand Inc. (SESOC), New Zealand Geotechnical Society Inc., Ministry of Business, Innovation and Employment, Earthquake Commission. The Seismic Assessment of Existing Buildings (the Guidelines), Part C—Detailed Seismic Assessment; <http://www.eq-assess.org.nz/>
- Petrone C, Magliulo G, Manfredi G (2015) Seismic demand on light acceleration-sensitive nonstructural components in European reinforced concrete buildings. *Earthq Eng Struct Dyn* 44:1203–1217
- Rodriguez D, Perrone D, Filiatrault A, Brunesi E (2021) A probabilistic strong floor motion duration model for seismic performance assessment of non-structural building elements. *Earthq Eng Struct Dyn* 50:4161–4179
- Senaldi I, Magenes G, Penna A, Galasco A, Rota M (2014) The effect of stiffened floor and roof diaphragms on the experimental seismic response of a full-scale unreinforced stone masonry building. *J Earthquake Eng* 18(3):407–443. <https://doi.org/10.1080/13632469.2013.876946>
- Senaldi IE, Guerrini G, Comini P, Graziotti F, Penna A, Beyer K, Magenes G (2020) Experimental seismic performance of a half-scale stone masonry building aggregate. *Bull Earthq Eng* 18(2):609–643

- Sivori D, Lepidi M, Cattari S (2021) Structural identification of the dynamic behavior of floor diaphragms in existing buildings. *Smart Struct Syst* 27(2):173–191
- Sullivan TJ, Calvi PM, Nascimbene R (2013) Towards improved floor spectra estimates for seismic design. *Earthq Struct* 4(1):109–132
- Spina D, Lamonaca B (1998). Strengthening assessment of building using ambient vibration tests. In: *Proceedings of the 11th European Conference on Earthquake Engineering*, Paris, France
- Surana M, Pisode M, Singh Y, Lang DH (2018) Effect of URM infills on inelastic floor response of RC frame buildings. *Eng Struct* 175:861–878
- Vukobratović V, Fajfar P (2016) A method for the direct estimation of floor acceleration spectra for elastic and inelastic MDOF structures. *Earthq Eng Struct Dyn* 45:2495–2511
- Vukobratović V, Fajfar P (2017) Code-oriented floor acceleration spectra for building structures. *Bull Earthq Eng* 15(7):3013–3026

**Publisher's Note** Springer Nature remains neutral with regard to jurisdictional claims in published maps and institutional affiliations.